

**3-D FREE SURFACE FLOW MODELING
OF A CHANNEL CONFLUENCE USING
OPENFOAM**

BY

MUHAMMAD KASHIF JAWAD

00000277588



This thesis is submitted in partial fulfillment of the requirements of the degree of

MASTER OF SCIENCE

IN

WATER RESOURCES ENGINEERING AND MANAGEMENT

NUST INSTITUTE OF CIVIL ENGINEERING (NICE)

SCHOOL OF CIVIL AND ENVIRONMENTAL ENGINEERING (SCEE)

NATIONAL UNIVERSITY OF SCIENCES AND TECHNOLOGY (NUST)

ISLAMABAD, PAKISTAN

2021

1

This is to certify that the

Thesis titled

**3-D FREE SURFACE FLOW MODELING
OF A CHANNEL CONFLUENCE USING
OPENFOAM**

Submitted By

MUHAMMAD KASHIF JAWAD

00000277588

Has been accepted in partial fulfillment of the requirements towards the award of the
degree of

Master of Science

IN

Water Resources Engineering and Management

(2021)

Dr. Sajjad Haider

Associate Professor

NUST Institute of Civil Engineering (NICE)

School of Civil and Environmental Engineering (SCEE)

National University of Sciences and Technology (NUST)

THESIS ACCEPTANCE CERTIFICATE

Certified that final copy of MS thesis written by Mr. Muhammad Kashif Jawad, Registration No 00000277588, of MS Water Resources Engineering and Management 2018 Batch (NICE) has been vetted by undersigned, found completed in all respects as per NUST Statutes/Regulations, is free of plagiarism, errors, and mistakes and is accepted as partial fulfillment for award of MS/MPhil degree. It is further certified that necessary amendments as pointed out by GEC members of the scholar have been incorporated in the said thesis.

Signature _____

Name of Supervisor: Dr. Sajjad Haider

Date: _____

Signature (HoD) _____

Date _____

Signature (Dean/Principal) _____

Date: _____

ACKNOWLEDGEMENT

*All acclamations and appreciations are for **Almighty Allah**, who bestowed mankind with knowledge and wisdom, and granted him vigilance on earth.*

*I would like to pay my sincere and deepest gratitude to my supervisor **Dr. Sajjad Haider (NICE, NUST)** for believing in me to complete my research work. His important guidance, innovative suggestions and kind behavior were source of motivation during the study. I am grateful to all my teachers who taught me throughout my academic career and for their kind support.*

*I am grateful to **Dr. Hamza Farooq Gabriel**, my thesis committee member and HoD WRE & M for his continuous support.*

*I express my utmost gratitude to GEC members **Mam Ammara Mubeen** for their valuable help, technical acumen and moral support.*

*I would also like to pay my gratitude to my colleague **Mr. Mohsin Raza** for his thorough cooperation and guidance.*

It would not be possible to write MS thesis without the help and support of my loving mother and supportive siblings who have given me their unequivocal support throughout, for which my mere expressions of thanks do not suffice.

Abstract

Natural rivers usually have a main channel and a few tributaries. A confluence is the meeting of a tributary and the main channel. A typical phenomenon in many hydraulic engineering problems is the confluence of two streams. Natural river networks, water treatment plants, and fish passage conveyance systems are typical examples. Confluence hydrodynamics is particularly complicated since there are several factors affecting stream characteristics at the confluence such as geometric factors and flow parameters. Although there are several hydraulic problems with open channel confluences, only limited study has been made to deal with this point. Most research is focused on field experiments or experimental studies, and few mathematical models have been developed. This paper is aimed at building a collection of data which entirely explains the complicated, Flow conditions in the open channel junction in three-dimensions. The presented data set consists of 3D measurements of the velocity and turbulence, along with a water surface mapping in the immediate vicinity of the channel junction. In this analysis, a 90° sharp-edged junction of the same size channel was focused. The OpenFOAM CFD tool was used for simulation. Multiphase, InterFoam solver and the k- ω SST turbulence model was used for turbulence modelling. Volume of Fluid (VOF) method was used which captured the free water surface as well. After that, the simulation results are compared to the experimental results of the (Weber, Schumate et al. 2001). The main aim of the study is to introduce a 3D numerical model OpenFOAM CFD tool validation with excellent test information. The model is validated using only one flow condition of the (Weber, Schumate et al. 2001) test results. A strong understanding is accomplished between the experimental reports and the computational model.

TABLE OF CONTENT

Chapter 1	15
INTRODUCTION	15
1.1 Overview	15
1.2 Goals	17
1.2.1 General goal	17
1.2.2 Specific goals	18
1.3 Dissertation Structure	18
Chapter 2	19
LITERATURE REVIEW	19
2.1 Theory	19
2.2 Open-channel confluences	19
2.3 Conservation laws of fluid motion	22
2.4 Three-dimensional mass conservation	22
2.5 Three-dimensional Momentum equation	24

2.6 Navier-Stokes Newtonian fluid equations.....	26
2.7 Volume of Fluid Method (VOF)	28
2.8 Turbulence	28
2.8.1 RANS Turbulence models	30
2.8.2 Law of the wall	34
2.9 Computational Fluid Dynamics (CFD) modeling	36
2.9.1 Computational Fluid Dynamics (CFD) in industry.....	36
2.9.2 Computational Fluid Dynamics (CFD) in confluences.....	38
2.9.3 Open Field Operations and Manipulation (OpenFOAM)	48
Chapter 3	51
METHODOLOGY	51
3.1 The 3D Open-Source Model OpenFOAM	51
3.2 Volume of Fluid Method (VOF)	52
3.3 Solution Domain.....	52
3.4 Geometry	53
3.5 Boundary Conditions	54

3.6 Modeling with OpenFOAM	55
3.6.1 Preprocessing	55
3.6.2 0 Folder (Initial Field Values).....	56
3.6.3 Constant Directory	57
3.6.4 System Directory.....	58
3.6.5 Processing	60
3.6.6 Post Processing	61
3.7 Study case	62
Chapter 4	66
RESULTS AND DISCUSSION	66
4.1 Assessment of Velocity vectors in Plan view	66
4.2 Longitudinal velocities	67
4.2.1 Comparison of Vertical profiles of Streamwise Velocity	67
4.2.2 Assessment of velocity variations in plan view	70
4.2.3 Velocity variation assessment in cross-section.....	73
4.3 Free-Surface Treatment	76
4.3.1 Comparison of Water-Surface Elevation	76

4.3.2 Water surface elevation profiles	78
4.4 Turbulent Kinetic Energy	79
Chapter 5	81
CONCLUSIONS AND RECOMMENDATIONS.....	81
5.1 Conclusions	81
5.2 Recommendations	82
REFERENCES	84

LIST OF ABBREVIATIONS AND SYMBOLS

Abbreviation	Meaning
1D, 2D or 3D	One, Two or Three dimensional
ADV	Acoustic Doppler Velocimeter
CFD	Computational Fluid Dynamics
DNS	Direct Numerical Simulation
F_r	Froude number
FVM	Finite Volume Method
G	Gravitational acceleration
H_o	Tailwater depth
HOL	Height of Liquid
I	Turbulence intensity
K	Turbulent kinetic energy
k- ω	K Omega Turbulence Model
k- ω SST	k- ω Shear Stress Transport Model
k- ϵ	K Epsilon Turbulence model
LES	Large Eddy Simulation
NS	Navier-Stokes
Nut	Turbulent viscosity
Omega	Specific dissipation rate
OpenFOAM	Open Field Operations and Manipulation
P_rgh	Pressure divided by density
PIMPLE	Pressure Implicit Momentum with Pressure Linked Equations
PISO	Pressure Implicit with Splitting of Operator
POR	Porosity Concept
q^*	Flow ratio (Q_m / Q_t)
Q_b	Branch channel inflow

Q_m	Main channel inflow
Q_t	Outflow
RANS	Reynolds-Averaged Navier-Stokes
RL	Rigid Lid
RMSE	Root Mean Square Error
RSM	Reynolds Stress Model
SIMPLE	Semi-Implicit Method for Pressure Linked Equations
SSIIM	Sediment Simulation in Intakes with Multiblock
U	U Velocity in x-direction
V	Velocity in y-direction
VOF	Volume of Fluids method
W	Velocity in z-direction

LIST OF TABLES

Table 2. 1	Extra transport equations classify the utmost popular turbulence models.	33
Table 3. 1	Summary of Initial conditions.....	57
Table 3. 2	Physical properties of Water and Air	57
Table 3. 3	Numerical schemes adopted.....	60
Table 4. 1	Comparison of Separation zone dimensions	70

LIST OF FIGURES

Figure 2.1. Schematic diagram for $q^* = 0.250$ (Weber, Schumate et al. 2001).....	20
Figure 2.2. Mass enters and exits the fluid element. (Versteeg and Malalasekera 2007)	23
Figure 2.3. Components of stress in the x-direction (Versteeg and Malalasekera 2007)	25
Figure 2.4. Longitudinal view diagram of transition processes over a flat plate in boundary layer flow (Frei 2013)	29
Figure 2.5. In a Turbulent flow typical calculation of a point velocity (Versteeg and Malalasekera 2007)	31
Figure 2.6. Near a solid boundary, a typical mean velocity profile. (Frei 2013).....	34
Figure 2.7. (a) Plan view Dimensional longitudinal (lengthwise) velocity (u^*) projections at ($z/W = 0.278$) and (b) cross-sectional velocity projection at ($x/W = -2$) (Weber, Schumate et al. 2001).....	40
Figure 2.8. Exp. Streamwise Velocities at $x/W = -2$ (Weber, Schumate et al. 2001)..	41
Figure 2.9. Velocity vectors at Cross-section ($x = -2$) (Weber, Schumate et al. 2001)	41
Figure 2.10. Exp. Water-surface mapping (Weber, Schumate et al. 2001)	41
Figure 2.11. Distribution of TKE ($z/W = 0.278$) (Weber, Schumate et al. 2001)	42
Figure 2.12. Profiles of vertical streamwise velocities at $x/W = 1$ from (Lira 2014) ..	45
Figure 2.13. Profiles of vertical streamwise velocities at $y/W = -1$ from (Lira 2014).	46
Figure 2.14. Profiles of vertical streamwise velocities at $x/W = 0$ from (Lira 2014) ..	46
Figure 2.15. Profiles of vertical streamwise velocities at $x/W = -1$	46
from (Lira 2014).....	46
Figure 2.16. Profiles of vertical streamwise velocities at $x/W = -2$	47
from (Lira 2014).....	47
Figure 2.17. Profiles of vertical streamwise velocities at $x/W = -6$	47
from (Lira 2014).....	47

Figure 2.18. Structure of the OpenFOAM case directory (OpenFOAM 2014).....	49
Figure 3.1. BlueCFD Terminal Interface	51
Figure 3.2. 2D Representation of Domain	52
Figure 3.3. Plan view of coarser mesh	53
Figure 3.4. Basic Structure for OpenFOAM Directories	56
Figure 3.5. ParaView Interface	62
Figure 3.6. Layout of experimental flume	64
Figure 3.7. Position for gathering of data in a cross-section (Weber, Schumate et al. 2001)	64
Figure 3.8. Stations for gathering of data for each cross-section (Weber, Schumate et al. 2001)	65
Figure 4.1. Velocity vectors plan view comparison at $z/W = 0.278$	67
Figure 4.2. Comparison of streamwise velocities at $x/W = 1$	68
Figure 4.3. Comparison of streamwise velocities at $x/W = 0$	68
Figure 4.4. Comparison of streamwise velocities at $x/W = -1$	69
Figure 4.5. Comparison of streamwise velocities at $x/W = -2$	69
Figure 4.6. Comparison of streamwise velocities at $x/W = -6$	70
Figure 4.7. Plan view comparison of u velocity distribution at $z/W = 0.278$	71
Figure 4.8. Plan view comparison of u velocity distribution at $z/W = 0.014$	72
Figure 4.9. Cross-section comparison of u velocity distribution at $x/W = 0$	73
Figure 4.10. Cross-section comparison of u velocity distribution at $x/W = -1$	74
Figure 4.11. Cross-section comparison of u velocity distribution at $x/W = -1.67$	75
Figure 4.12. Cross-section comparison of u velocity distribution at $x/W = -7$	76
Figure 4.13. Water Surface Contours Comparison	77
Figure 4.14. Water Surface Mapping Comparison	78
Figure 4.15. Comparison of water surface elevation profiles in the main channel, Blue line is experimental data by (Weber, Schumate et al. 2001) and Red line is present calculation	79
Figure 4.16. Comparison of Turbulent Kinetic Energy at $z/W = 0.278$	80

INTRODUCTION

1.1 Overview

In human nature the ability to comprehend and forecast natural phenomena is obviously inherent. Since prehistoric days, People have been studying nature and developing mathematical models of some of its characteristics for a long time. A computational model is designed to make the interpretation, description, quantification, visualization, and simulation of a specific component or function of the planet simpler. Whenever it refers to hydraulic structure design, identification of flow parameters is not really an intention; it is a necessity.

Structures can be designed using four different modelling resources in hydraulic engineering, as well as other fields: Simple calculations using analytical (hypothetical) calculations, computations using empirical (investigational) calculations, computational replicas, and physical models on a tiny level. First two techniques are generally used to construct a conceptual design that incorporates all of a structure's important dimensions, when a greater analysis of flow pattern is needed, the last two are used to design structure's design and protection.

Given some boundary and initial conditions, a scientific model uses numerical techniques and procedures to work out mathematical calculations with goal of capturing a physical process in geometry. Companies and everyday citizens are now using computational models constructed years earlier to model challenging fluid flows, thanks to technical advancements in computational resources. As a result, computational simulations have been an effective method for reducing total project costs before constructing proper physical models. The implementation of hydraulic systems as well as the evaluation of final requirements in their configuration numerical models are

specifically used in certain smaller projects where building physical models is not commercially feasible.

A broad array of computational methods and there have been developed turbulence model to describe the vast array of flow forms found in nature as well as in industry. Even so, there seems to be a discrepancy between the models' expected potential and the certainty of their accuracy in various scenarios. As a result, users may feel more secure when choosing settings if there are more research cases reported in the documentation.

It is necessary to note that the use of powerful software does not guarantee successful modelling. It is preferable that the physical phenomenon should be focused, such as projected flow patterns, and even the computational model incorporating equations and numerical methods. In reality, in the hands of a novice consumer, a computational model, no matter how stable, has the potential to cause significant damage. As a consequence, this project emerged from the author's desire to gain familiarity with the subject and become acquainted with its complexities and limitations.

A 90° open-channel confluence was used as the study case. The following are the reasons for this choice: Fluid flow is a very complex phenomenon and the level of work carried out on this topic is very rare especially in Pakistan. Confluence is a very common, simplistic geometric hydraulic structure, facilitates simulation, reproduces a dynamic, fully 3D flow.

OpenFOAM, the free to use and open-source computational fluid dynamics (CFD) software was utilized in this analysis. The programme was widely used by academics in particular and its no costs and the large variety of resources and methods could be credited to it. Nevertheless, there are just a few studies in the open channel flows and certainly none on confluence using this programme.

Natural rivers usually have a main channel and a few tributaries. A confluence is the meeting of a tributary and the main channel. A typical phenomenon in many hydraulic engineering problems is the confluence of two streams. Natural river networks, water

treatment plants, and fish passage conveyance systems are typical examples. Confluence hydrodynamics is particularly complicated since there are several factors affecting stream characteristics at the confluence. A number of geometrical factors, for example height, shape, incline and angle between two channels can be depicted as one set of factors. There are various mixtures of these four variables are possible. Flow parameters including the, for example, downstream flow Froude number, the roughness of the channel, the discrepancy in fluid characteristics as well as the ratio between the two flux channels form a second arrangement of boundaries. Although there are several hydraulic problems with open channel confluences, only limited study has been made to deal with this point. Most research is focused on field experiments or experimental studies, and few mathematical models have been developed.

This paper is aimed at building a collection of data which entirely explains the complicated, Flow conditions in the open channel junction in three-dimensions. The presented data set consists of 3D measurements of the velocity and turbulence, along with a water surface mapping in the immediate vicinity of the channel junction. In this analysis, a 90° sharp-edged junction of the same size channel was focused.

1.2 Goals

The research topic supporting this thesis represents a very practical engineering challenge. This paper was not meant to show any new numeric modelling outcomes. The goal is instead to carefully investigate the capacities of freely available, open sourced CFD package while taking into consideration previous model applications with the same subject, in order to make a contribution to the scientific frontier.

1.2.1 General goal

The primary objective of this analysis has been to establish and test the capability of a three-dimensional numerical model to replicate the flux features accurately by comparing the findings with recorded experimental data 90° open channel confluence.

The geometry and mesh are created, as well as all of the necessary files, such as the initial and boundary conditions were created. The OpenFOAM CFD tool was used for simulation, and the $k-\omega$ SST turbulence model was used for turbulence modelling. After that, the simulation results are compared to the experimental results of the (Weber, Schumate et al. 2001)

1.2.2 Specific goals

- Simulate flow in a T-Shape Channel using a 3D model.
- Compare the simulated and observed variables.
- Discuss and correlate the parameters applying different mesh density and turbulence models.
- To test OpenFOAM's competences and user friendliness.

1.3 Dissertation Structure

The Introduction, History, Thesis Objective, Scope of Research, and Dissertation are all included in Chapter 1.

Theory, governing equations, a brief discussion of various turbulence models, and a literature review comprise Chapter 2.

Chapter 3 covers the methodology of the research in detail which includes OpenFOAM, Preprocessing, Processing, Postprocessing and Case Study.

Chapter 4 discusses the results in detail.

Chapter 5 encompasses conclusions and recommendations.

LITERATURE REVIEW

2.1 Theory

The aim of this first subchapter is to go through some of the background information on confluence research and how its models were created. In the following two subchapters, the system of equations of fluid motion, along with essential characteristics of turbulence models and turbulent flow, are discussed. This provides a mathematical foundation for a general-purpose Computational Fluid Dynamics (CFD) model. Finally, an assessment of the literature on the use of CFD in industry and in confluence studies is conducted.

2.2 Open-channel confluences

Confluences can be seen in various surrounding environment. River junctions, man-made and natural open-channels present diverse flow features controlled by a large number of criterions in waterways in the countryside and in municipal water networks. Although the effect of the low slope and the boundary roughness have a little effect on the near-flux field of a junction, it is not possible to implement technical calculations in a straight channel to the systematic hydraulic treatment of a confluence.

90° open channel confluence was studied by (Weber, Schumate et al. 2001) in his laboratory. Everywhere the width of the channel was similar. The major length of the channel was 21.95 meters, and the length of the branch channel was 3.66 meters. And the channel height was 0.51 meters. 3D data on velocity, surface water elevation data, and turbulent kinetic energy data were given. Which was very helpful for understanding the junction flow and also our CFD model for validation.

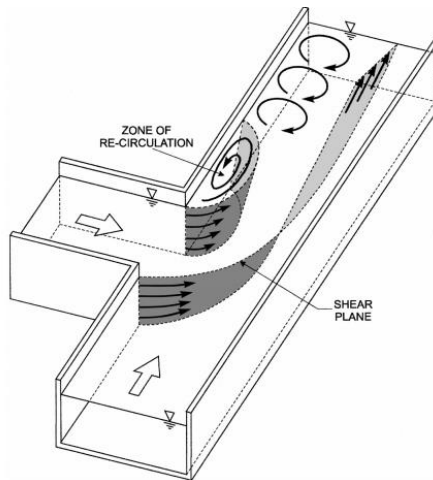


Figure 2.1. Schematic diagram for $q^* = 0.250$ (Weber, Schumate et al. 2001)

The flow configuration near the junction for such subcritical stream flow can be seen in Figure 2.1. The flow patterns have the following main characteristics: an inner recirculating separating zone; elevated turbulence and lowered water level just below the branch contribution; the resulting higher speed velocities contracting segment; a stagnating point located near the upstream edge; a helical circular path downstream channel because the lateral channel flow is reflected against the junction-opposition.

(Taylor 1944) being the first, addressed his research on a basic junction flow including the observations in subcritical conditions of 45° and 135° intersections of manmade rectangular channels as well as a momentum analysis that resulted in a profound equation for the depth ratio among downstream and upstream branches of the channel.

Later On, (Webber and Greated 1966) for subcritical conditions presented predictive equations for the depth ratio by relating various flow variables (better accuracy than Taylor (1944)). They also used the conformal mapping approach to present energy loss relationships and theoretical flow patterns.

The features and degree of channel deformation at the natural confluence of the Kura river are further investigated by (Mamedov 1989). The same researcher suggested analytical methods to calculate plan of the currents, channel stability, and useful contracted region parameters (location, mean velocity as well as depth) and the separation region (extent and thickness). Furthermore, laboratory studies were performed in a rectangular flume to study more closely the effect of the confluence angle and the linkage of discharges releases at the confluence.

Centered on laboratory experiments performed in a subcritical confluence (Gurram, Karki et al. 1997) proposed coefficients for momentum correction, the depth ratios as well as lateral wall pressure force in the lateral branch and upstream branch. A rational method for the lateral branch's momentum contribution was also proposed and extended to the estimation of a backwater effect over a simple junction.

At the junctions, in several One-dimensional computational model's mass conservation as well as the momentum conservation concepts are applied for an open channel network. Due to the very difficult of measuring velocity head and energy loses, the continuity of the discharge and water surface altitude would actually decrease in equality with internal boundary conditions. HEC-RAS another computational model which is one-dimensional, free and perhaps the most widely used software, also allows us to apply momentum conservation method rather than energy conservation, but this model also implies that the upstream depths are equivalent. Later on, (Shabayek, Steffler et al. 2002) created one-dimensional model which does not presume equivalent upstream depths by implementing mass conservation and momentum conservation and taking into account an enhanced collection of internal boundary conditions to fill this void.

In open channel networks, when the objective is to reproduce approximation of the free surface profiles, the analytical models and empirical models developed by (Taylor 1944, Webber and Greated 1966, Gurram, Karki et al. 1997, Shabayek, Steffler et al. 2002) are very helpful to be implemented in one-dimensional numerical models.

2.3 Conservation laws of fluid motion

The equations given in this subtopic are three-dimensional assessment of the classical governing fluid motion equations. This subsection focuses primarily on the contents of chapter 2 of (Versteeg and Malalasekera 2007). The viscous stresses, pressure, scalar velocities in the x-direction, y-direction, and z-direction, density, pressure, and velocity vectors are all represented by the letters τ , p , u , v , w , ρ , and u respectively. The equations that govern the fluid flow are the mathematical expression of physics conservational laws.

- A fluid mass cannot be produced or destroyed - resulting in the mass conservation equation.
- Total forces acting on the fluid particle are equal to rate of momentum change - resulting in the momentum equation. (second law of Newton)
- The rate of energy changing is the same as the sum of the heat addition rate and the working rate of a fluid object (the first law of thermodynamics) – resulting in the energy equation.

Incompressible fluids are gases and liquids moving at low speeds, according to (Versteeg and Malalasekera 2007). Without density variation, there is no relationship between the mass conservation, momentum equations, and energy equations. Momentum equations and mass conservation are also sufficient to solve the flow field. The energy equation is not discussed because this is the issue examined in this assessment and temperature of the water was kept stable.

2.4 Three-dimensional mass conservation

The mass balance of a fluid element is the first step in obtaining the equation of conservation of mass equation:

Rate of mass increase in fluid element is equal to Net rate of mass flow through fluid element.

The fluid variable's mass increases at the following rate:

$$\frac{\partial}{\partial t}(\rho \delta x \delta y \delta z) = \frac{\partial \rho}{\partial t} \delta x \delta y \delta z \quad 2.1$$

As depicted in Figure 2.2, When area, velocity component and the density that is normal to the face is multiplied, the mass flow rate through an element face is calculated.

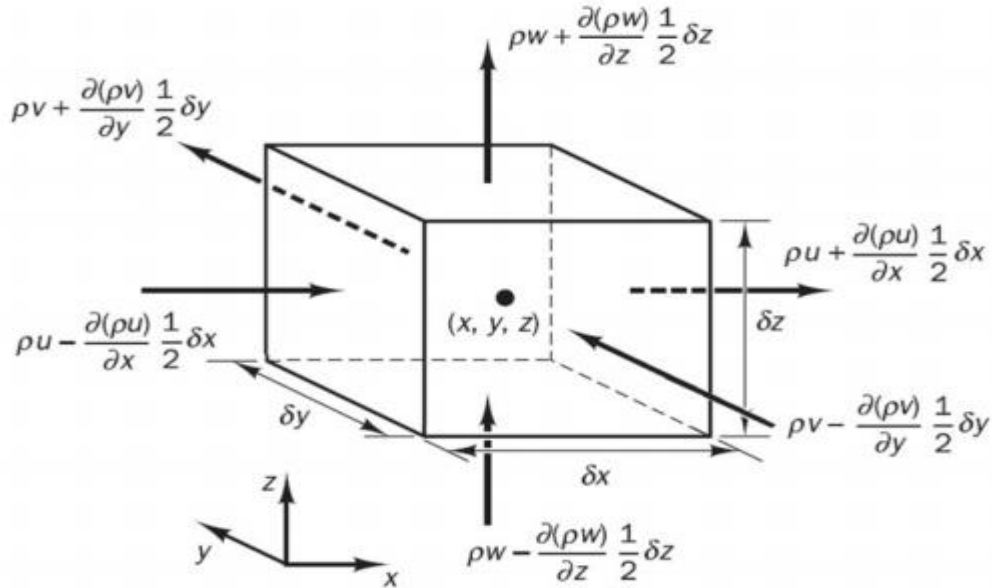


Figure 2.2. Mass enters and exits the fluid element. (Versteeg and Malalasekera 2007)

The following three-dimensional, unsteady continuity equation or mass conservation equation is achieved at such a stage in a compressible fluid when all of the components are added together, assembled and then equating them to equation 2.1.:

$$\frac{\partial \rho}{\partial t} + \frac{\partial(\rho u)}{\partial x} + \frac{\partial(\rho v)}{\partial y} + \frac{\partial(\rho w)}{\partial z} = 0 \quad \text{or} \quad \frac{\partial \rho}{\partial t} + \text{div}(\rho \mathbf{u}) = 0 \quad 2.2$$

In case of incompressible fluids, for example, when water is flowing at a channel junction, the density is constant as investigated in this report, then equation 2.2 will become:

$$\frac{\partial u}{\partial x} + \frac{\partial v}{\partial y} + \frac{\partial w}{\partial z} = 0 \quad \text{or} \quad \text{div } \mathbf{u} = 0 \quad 2.3$$

2.5 Three-dimensional Momentum equation

The second law of Newton states:

Rate of fluid particle momentum increase is equal to Sum of all fluid particle forces.

The increase rate of a fluid particle per unit volume of x-momentum is:

$$\rho \left(\frac{\partial u}{\partial t} + u \frac{\partial u}{\partial x} + v \frac{\partial u}{\partial y} + w \frac{\partial u}{\partial z} \right) = \rho \frac{\partial u}{\partial t} + \text{div}(u\mathbf{u}) = \rho \frac{Du}{Dt} \quad 2.4$$

Similarly increasing rates in both the y- direction and in the z-direction can be found. Forces that are acting on a fluid particle are of two types: body forces which include Coriolis, gravity, centrifugal and electromagnetic forces and the surface forces comprises of viscous and pressure forces. Mostly in momentum equation, it is standard practice to illustrate the influences caused by surface forces as independent terms and to incorporate the influences of body forces as core terms. The nine components of viscous stresses and pressure defines the fluid element's state of stress as depicted in Figure 2.3a and 2.3b.

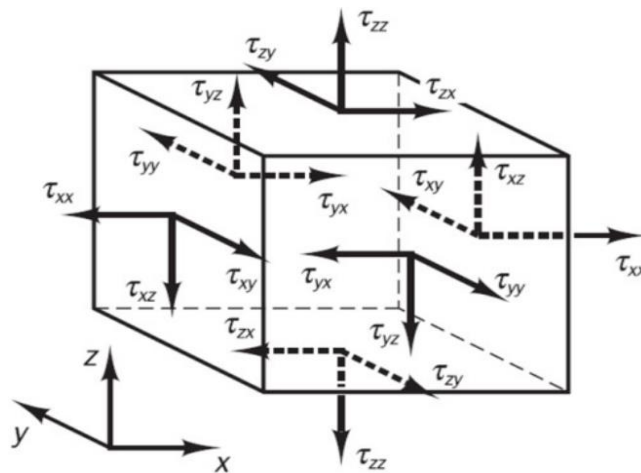


Figure 2.3a. Components of stress on three sides of a fluid element (Versteeg and Malalasekera 2007)

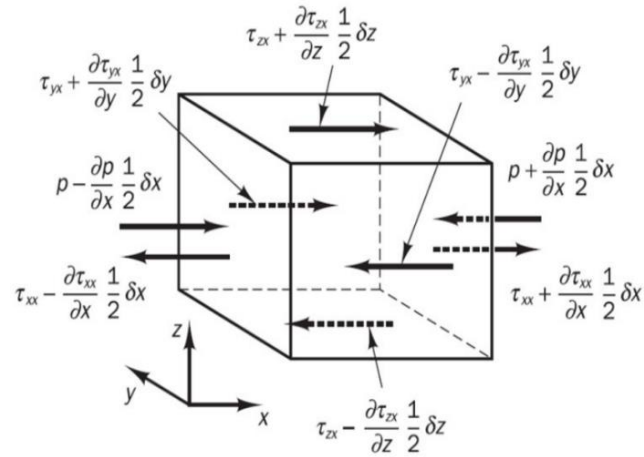


Figure 2.3. Components of stress in the x-direction (Versteeg and Malalasekera 2007)

The force produced by a surface stress is defined by the product of stress and area. In the x-direction, the cumulative force applied on the fluid by such surface stresses per unit volume is equivalent to:

$$\frac{\partial(-p+\tau_{xx})}{\partial x} + \frac{\partial(\tau_{yx})}{\partial y} + \frac{\partial(\tau_{zx})}{\partial z} \quad 2.5$$

Without going into great detail about body forces as Coriolis forces and gravity forces, their combined influence should be taken into account by describing a source S_{Mx} of x-momentum per unit time per unit volume.

When equation 2.4 is set equivalent to equation 2.5 and by adding S_{Mx} , yields momentum equation x-component:

$$\rho \frac{Du}{Dt} = \frac{\partial(-p+\tau_{xx})}{\partial x} + \frac{\partial(\tau_{yx})}{\partial y} + \frac{\partial(\tau_{zx})}{\partial z} + S_{Mx} \quad 2.6$$

In the same way momentum equation y-component is obtained:

$$\rho \frac{Dv}{Dt} = \frac{\partial(\tau_{xy})}{\partial x} + \frac{\partial(-p+\tau_{yy})}{\partial y} + \frac{\partial(\tau_{zy})}{\partial z} + S_{My} \quad 2.7$$

and the momentum equation's z-component is given by:

$$\rho \frac{Dv}{Dt} = \frac{\partial(\tau_{xz})}{\partial x} + \frac{\partial(\tau_{yz})}{\partial y} + \frac{\partial(-p + \tau_{zz})}{\partial z} + S_{Mz} \quad 2.8$$

2.6 Navier-Stokes Newtonian fluid equations

The viscous stress components τ_{ij} are still unknowns in the governing equations. For fluid flows the most effective types of the conservation equation for the viscous stresses τ_{ij} are achieved by adding an appropriate model. Many liquids and all gases behave in an isotropic manner. In such situations, the viscous stresses can be represented as a function of the local deformation rate or strain rate, which is made up of three linear elongating deformation components and has nine components in three dimensions:

$$S_{xx} = \frac{\partial u}{\partial x} \quad S_{yy} = \frac{\partial v}{\partial y} \quad S_{zz} = \frac{\partial w}{\partial z} \quad 2.9$$

In isotropic fluids, there are six shearing linear deformation components that are independent:

$$S_{xy} = S_{yx} = \frac{1}{2} \left(\frac{\partial u}{\partial y} + \frac{\partial v}{\partial x} \right) \quad S_{xz} = S_{zx} = \frac{1}{2} \left(\frac{\partial u}{\partial z} + \frac{\partial w}{\partial x} \right) \quad S_{zy} = S_{yz} = \frac{1}{2} \left(\frac{\partial w}{\partial y} + \frac{\partial v}{\partial z} \right) \quad 2.10$$

The volumetric deformation is given by:

$$\frac{\partial u}{\partial x} + \frac{\partial v}{\partial y} + \frac{\partial w}{\partial z} = \text{div } \mathbf{u} \quad 2.11$$

The rates of deformation in a Newtonian fluid are proportional to viscous stresses. Two proportionality constants are involved in Newton's three-dimensional viscosity law for compressible flows: firstly viscosity μ (dynamic), is related to linear deformations, and the second viscosity λ , is related to stresses to volumetric deformations, typically estimated to $\lambda = \frac{2}{3}\mu$, according to (Schlichting 1979). The nine viscous stress components are:

$$\tau_{xx} = 2\mu \frac{\partial u}{\partial x} + \lambda \text{div } \mathbf{u} \quad \tau_{yy} = 2\mu \frac{\partial v}{\partial y} + \lambda \text{div } \mathbf{u} \quad \tau_{zz} = 2\mu \frac{\partial w}{\partial z} + \lambda \text{div } \mathbf{u}$$

$$\tau_{xy} = \tau_{yx} = \mu \left(\frac{\partial u}{\partial y} + \frac{\partial v}{\partial x} \right) \quad \tau_{xz} = \tau_{zx} = \mu \left(\frac{\partial u}{\partial z} + \frac{\partial w}{\partial x} \right) \quad \tau_{yz} = \tau_{zy} = \mu \left(\frac{\partial v}{\partial z} + \frac{\partial w}{\partial y} \right) \quad 2.12$$

In order to obtain the Navier-Stokes equations (for fluids having variable viscosity and that are compressible) simply substitute equation 2.12 into equations 2.6 and 2.8:

$$\begin{aligned} \rho \frac{Du}{Dt} &= -\frac{\partial p}{\partial x} + \frac{\partial}{\partial x} \left[2\mu \frac{\partial u}{\partial x} + \lambda \operatorname{div} \mathbf{u} \right] + \frac{\partial}{\partial y} \left[\mu \left(\frac{\partial u}{\partial y} + \frac{\partial v}{\partial x} \right) \right] + \frac{\partial}{\partial z} \left[\mu \left(\frac{\partial u}{\partial z} + \frac{\partial w}{\partial x} \right) \right] + S_{Mx} \\ \rho \frac{Dv}{Dt} &= -\frac{\partial p}{\partial y} + \frac{\partial}{\partial x} \left[\mu \left(\frac{\partial u}{\partial y} + \frac{\partial v}{\partial x} \right) \right] + \frac{\partial}{\partial y} \left[2\mu \frac{\partial v}{\partial y} + \lambda \operatorname{div} \mathbf{u} \right] + \frac{\partial}{\partial z} \left[\mu \left(\frac{\partial v}{\partial z} + \frac{\partial w}{\partial y} \right) \right] + S_{My} \\ \rho \frac{Dw}{Dt} &= -\frac{\partial p}{\partial z} + \frac{\partial}{\partial x} \left[\mu \left(\frac{\partial u}{\partial z} + \frac{\partial w}{\partial x} \right) \right] + \frac{\partial}{\partial y} \left[\mu \left(\frac{\partial v}{\partial z} + \frac{\partial w}{\partial y} \right) \right] + \frac{\partial}{\partial z} \left[2\mu \frac{\partial w}{\partial z} + \lambda \operatorname{div} \mathbf{u} \right] + S_{Mz} \end{aligned} \quad 2.13$$

Since the flow in this study is assumed to be incompressible, the mass conservation equation is $\operatorname{div} \mathbf{u} = 0$. In addition, the viscosity is believed to be constant. As a result, the Navier-Stokes equations can be reduced to:

$$\begin{aligned} \rho \frac{Du}{Dt} &= -\frac{\partial p}{\partial x} + \mu \left(\frac{\partial^2 u}{\partial x^2} + \frac{\partial^2 u}{\partial y^2} + \frac{\partial^2 u}{\partial z^2} \right) + S_{Mx} = -\frac{\partial p}{\partial x} + \mu \operatorname{div}(\operatorname{grad}(u)) + S_{Mx} \\ \rho \frac{Dv}{Dt} &= -\frac{\partial p}{\partial y} + \mu \left(\frac{\partial^2 v}{\partial x^2} + \frac{\partial^2 v}{\partial y^2} + \frac{\partial^2 v}{\partial z^2} \right) + S_{My} = -\frac{\partial p}{\partial y} + \mu \operatorname{div}(\operatorname{grad}(v)) + S_{My} \\ \rho \frac{Dw}{Dt} &= -\frac{\partial p}{\partial z} + \mu \left(\frac{\partial^2 w}{\partial x^2} + \frac{\partial^2 w}{\partial y^2} + \frac{\partial^2 w}{\partial z^2} \right) + S_{Mz} = -\frac{\partial p}{\partial z} + \mu \operatorname{div}(\operatorname{grad}(w)) + S_{Mz} \end{aligned} \quad 2.14$$

There are a lot of important similarities among the different equations, as shown by equations 2.2 and 2.14. Therefore, we can write a general incompressible fluid transport equation as follows:

$$\frac{\partial \phi}{\partial t} = \operatorname{div}(\phi \mathbf{u}) = \frac{1}{\rho} \operatorname{div} \left(\Gamma_\phi \operatorname{grad}(\phi) \right) + S_\phi \quad 2.15$$

This equation was defined by (Versteeg and Malalasekera 2007) as follow:

$$\begin{array}{ccccccc}
 \text{Rate of increase} & & \text{Net rate of flow of } \phi & & \text{Rate of increase of } \phi & & \text{Rate of increase of } \phi \\
 \text{of } \phi \text{ of fluid} & & \text{out of fluid element} & = & \text{due to diffusion} & + & \text{due to sources} \\
 \text{element (rate of} & + & \text{(convective term)} & & \text{(diffusion term)} & & \text{(source term)} \\
 \text{change term)} & & & & & &
 \end{array}$$

2.7 Volume of Fluid Method (VOF)

With air communicating with the fluid at the surface, open channel flow is often a multiphase flow in nature. Therefore, phase fraction of fluid in a control volume is given by the equation taken from (Kravchenko and Moin 2000).

$$\rho = \alpha\rho_1 + (1 - \alpha)\rho_2 \tag{2.16}$$

Where α and ρ_1 denote the volume fraction and density of phase 1 (water), respectively, and ρ_2 denotes the density of phase 2 (air). Since the fluid's density remains constant in the domain, the above equation becomes:

$$1 = \alpha_1 + (1 - \alpha_2) \tag{2.17}$$

The volume fraction is governed by the transport equation (Kravchenko and Moin 2000).

$$\frac{\partial \alpha}{\partial t} + \nabla \cdot \alpha u = \mu \nabla^2 \alpha \tag{2.18}$$

2.8 Turbulence

The adjacent layers of fluid flow are smooth and slide past each other in an organized manner, it is said to be laminar. This can be represented by values below the critical Reynold number according to the experiments on fluid system. The flow behavior becomes unpredictable and spontaneous as the Reynolds number rises above Re_{crit} , resulting in turbulent flow.

One of the causes of turbulence is velocity gradients, or velocity variations between adjacent layers. Figure 2.4 clearly illustrates the incoming laminar flow transitioning to

a completely developed turbulent flow. Viscous stresses tend to appear and velocities nearer to the plate decreases due to friction, resulting in the generation of TKE.

Turbulent variations often have a three-dimensional spatial character, according to (Versteeg and Malalasekera 2007). Rotational flow configurations also generally known as turbulent eddies, are viewed in turbulent flow visualizations. Through diffusion, these vortices are capable of exchanging and transporting mass, momentum, and heat. It differs in sizes from quite massive eddies to very small ones, depending on the size of the shear flow that helps create the structures of primary vortex.

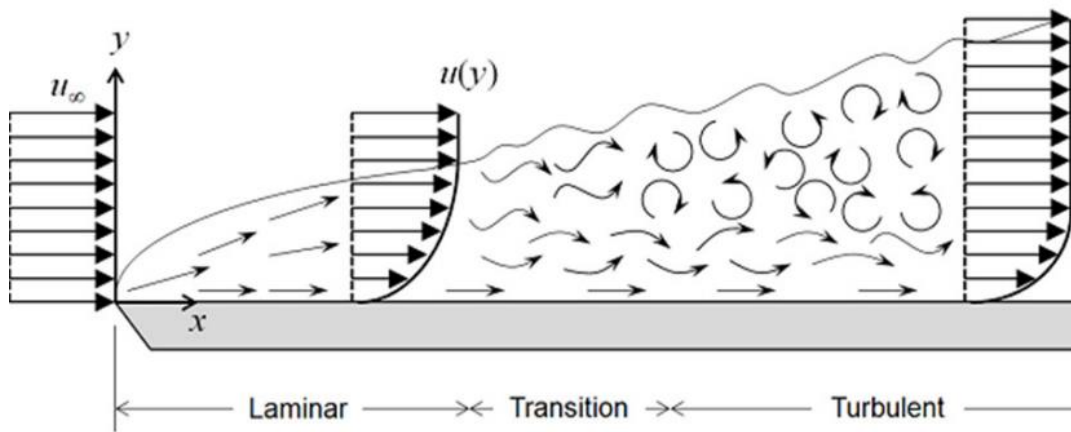


Figure 2.4. Longitudinal view diagram of transition processes over a flat plate in boundary layer flow (Frei 2013)

As a result of the break-up mechanism, a process known as the energy cascade, kinetic energy is transmitted from bigger to tinier structures. As tinier eddies have local Reynolds number equal to 1, indicating that the viscous forces and inertial forces strength are of equal magnitude. The bigger eddies are the more energy-efficient because they are driven by intensive engagements with the mean flow. Research is done in opposition to the behavior of at these smaller scale viscous stresses, allowing energy from small-scale eddy motions to be drained away and transformed into thermal internal energy. As a result, the more energy is dissipated when the flow is more turbulent.

Flows with low Reynolds number, in the laminar regime, are fully defined by the Navier-Stokes equation and continuity equation, According to (Schlichting 1979). Analytically the simple laminar flows can be solved, whereas when dealing with flows that are in complex laminar regime without further approximations should be solved numerically with CFD techniques. Wherein turbulence is found, the flow, however, represents higher Reynolds numbers in maximum practical engineering situations. Fluid engineers in these situations need instruments that can accurately reflect the turbulence impacts. The following three types can be listed into turbulence models:

- Reynolds-Averaged Navier-Stokes (or RANS) turbulence models: The additional terms arising from the time averaging of the Navier-Stokes (NS) equations, which are attributed to turbulent fluctuations, are determined by classical models such as Reynolds Stress Model (RSM) and the k-Epsilon model.
- Large Eddy Simulation (or LES): Before calculations to control the action of larger eddies space filtering of the NS equations is used. The solution of unsteady equations is required, which will raise the computational costs, however Computational Fluid Dynamics (CFD) problems with complicated geometries have already been solved.
- Direct Numerical Simulation (or DNS): All turbulent velocity variations and the mean flow are calculated using Direct Numerical Simulation (DNS). Industrial flow computations became unsuitable due to the high cost of computational resources.

2.8.1 RANS Turbulence models

Even with imposed boundary conditions, motion in a turbulent flow regime is intrinsically unsteady, and velocity, as well as all other flow characteristics, differ in a spontaneous and disorderly fashion. When the velocity in a flow is calculated, at a time, the standard time series graph illustrated in Figure 2.5 is obtained.

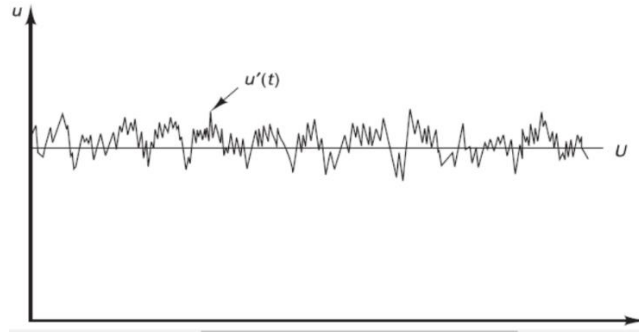


Figure 2.5. In a Turbulent flow typical calculation of a point velocity
(Versteeg and Malalasekera 2007)

The information of the turbulent flow fluctuations is not required for most engineering purposes, as only the mean properties are essential. A turbulent flow can be described in terms of the average values of flow features (defined in capital letter: Φ , P , W , V , U etc.) and their divergence (or fluctuation) from the mean (represented as: Φ' , p' , w' , v' , u' etc.). It is worth noting that the fluctuating component has a mean value = 0. In a general form:

$$\phi_t = \Phi + \phi'_t \quad 2.19$$

If we go back to Equation 2.3, $\text{div } u = \text{div } U$, which provides us the equation of continuity of mean flow:

$$\text{div } U = 0 \quad 2.20$$

In order to achieve RANS equations, NS equations (equation 2.14) are time averaged and fluctuating velocities supplementary terms are rearranged for incompressible flows.:

$$\frac{\partial U}{\partial t} + \text{div } (UU) = -\frac{1}{\rho} \frac{\partial P}{\partial x} + \nu \text{div}(\text{grad}(U)) + \frac{1}{\rho} \left[\frac{\partial(-\rho \overline{u'^2})}{\partial x} + \frac{\partial(-\rho \overline{u'v'})}{\partial y} + \frac{\partial(-\rho \overline{u'w'})}{\partial z} \right]$$

$$\frac{\partial V}{\partial t} + \text{div } (VV) = -\frac{1}{\rho} \frac{\partial P}{\partial y} + \nu \text{div}(\text{grad}(V)) + \frac{1}{\rho} \left[\frac{\partial(-\rho \overline{u'v'})}{\partial x} + \frac{\partial(-\rho \overline{v'^2})}{\partial y} + \frac{\partial(-\rho \overline{v'w'})}{\partial z} \right]$$

$$\frac{\partial W}{\partial t} + \text{div}(W\mathbf{W}) = -\frac{1}{\rho} \frac{\partial P}{\partial z} + v \text{div}(\text{grad}(W)) + \frac{1}{\rho} \left[\frac{\partial(-\rho \overline{u'w'})}{\partial x} + \frac{\partial(-\rho \overline{v'w'})}{\partial y} + \frac{\partial(-\rho \overline{w'^2})}{\partial z} \right] \quad 2.21$$

The so-called Reynolds stress is related to the fluctuating velocity terms, comprised of:

a) three normal stresses

$$\tau_{xx} = -\rho \overline{u'^2}, \quad \tau_{yy} = -\rho \overline{v'^2}, \quad \tau_{zz} = -\rho \overline{w'^2} \quad 2.22$$

b) and three shear stresses

$$\tau_{xy} = \tau_{yx} = -\rho \overline{u'v'}, \quad \tau_{xz} = \tau_{zx} = -\rho \overline{u'w'}, \quad \tau_{yz} = \tau_{zy} = -\rho \overline{v'w'} \quad 2.23$$

As per the Boussinesq hypothesis, deformation rates and Reynolds stresses are proportional to each other. It can be written as follows with the help of suffix annotation:

$$\tau_{ij} = -\rho \overline{u'_i u'_j} = \mu_t \left(\frac{\partial U_i}{\partial x_j} + \frac{\partial U_j}{\partial x_i} \right) - \frac{2}{3} \rho k \delta_{ij} = \mu_T S_{ij} - \frac{2}{3} \rho k \delta_{ij} \quad 2.24$$

With:

$$\delta_{ij} = 1 \quad \text{if } i = j,$$

and

$$\delta_{ij} = 0 \quad \text{if } i \neq j.$$

When equation 2.15 is derived, similar extra turbulent transport terms arise.

considering an arbitrary scalar quantity, $\phi(t) = \Phi + \phi'(t)$:

$$\frac{\partial \Phi}{\partial t} + \text{div}(\Phi \mathbf{U}) = \frac{1}{\rho} \text{div}(\Gamma_\Phi \text{grad}(\Phi)) + \frac{1}{\rho} \left[\frac{\partial(-\rho \overline{u'\phi'})}{\partial x} + \frac{\partial(-\rho \overline{v'\phi'})}{\partial y} + \frac{\partial(-\rho \overline{w'\phi'})}{\partial z} \right] + S_\Phi \quad 2.25$$

To close the system developed by mean flow equations 2.20, 2.21, and 2.25, turbulence models must be used to forecast scalar transport terms and Reynolds stresses. Table 2-1 lists the most popular RANS turbulence models, which are classified by the number of

supplementary transport equations that must be resolved in supplement to the RANS flow equations.

Table 2.1 Extra transport equations classify the utmost popular turbulence models.

No. of extra transport equations	Name
Seven-equation Turbulence Model	Reynolds Stress Equations Model (RSM)
Two-equation turbulence model	k-Epsilon ($k-\epsilon$) model
	k-omega ($k-\omega$) model
	Algebraic Stress Model (ASM)
Zero-equation turbulence model	Prandtl Mixing Length
One-equation turbulence model	Spalart-Allmaras (S-A) model

The flow in a confluence was calculated using a variant of the $k-\omega$ SST model in this study. As a result, it is briefly defined as:

2.8.1.1 The k-omega Shear Stress Transport (SST) model

The $k-\omega$ SST is the sole variant of the OpenFOAM's standard k-omega model. (Menter 1994) utilized the standard $k-\omega$ model and $k-\epsilon$ model to develop it. This model strives to combat the shortcomings of the k-omega standard model. The distinguishing factor is the manner wherein the model measures the turbulent viscosity to account for the transfer of the primary turbulent shear stress. To effectively measure the near-wall and far-field regions, this model includes a cross-diffusion parameter in the ω formula as well as a blending function. In near-wall locations, the blending mechanism activates the standard K-Omega model, while in locations farther from the walls, it activates the K-Epsilon-like model. This model is also capable of capturing the separation predictions

of flows. Because of these characteristics, the Shear Stress Transport model is quite robust than the standard model for a wider range of flows.

Equation for Turbulent Specific Dissipation rate:

$$\frac{D}{Dt}(\rho\omega) = \nabla \cdot (\rho D_\omega \nabla \omega) + \frac{\rho\gamma G}{\nu} - \frac{2}{3}\rho\gamma\omega(\nabla \cdot \mathbf{u}) - \rho\beta\omega^2 - \rho(F_1 - 1)CD_{k\omega} + S_\omega \quad 2.26$$

Equation for TKE:

$$\frac{D}{Dt}(\rho k) = \nabla \cdot (\rho D_k \nabla k) + \rho G - \frac{2}{3}\rho k(\nabla \cdot \mathbf{u}) - \rho\beta^*\omega k + S_k \quad 2.27$$

Using this equation turbulent viscosity is attained:

$$v_t = a_1 \frac{k}{\max(a_1\omega b_1 F_{23} S)} \quad 2.28$$

2.8.2 Law of the wall

The structure of turbulence and its flow conduct near solid walls vary significantly from free turbulent flows. As shown in Figure 2.6, the turbulent flow along solid boundaries are divided into four distinct regions:

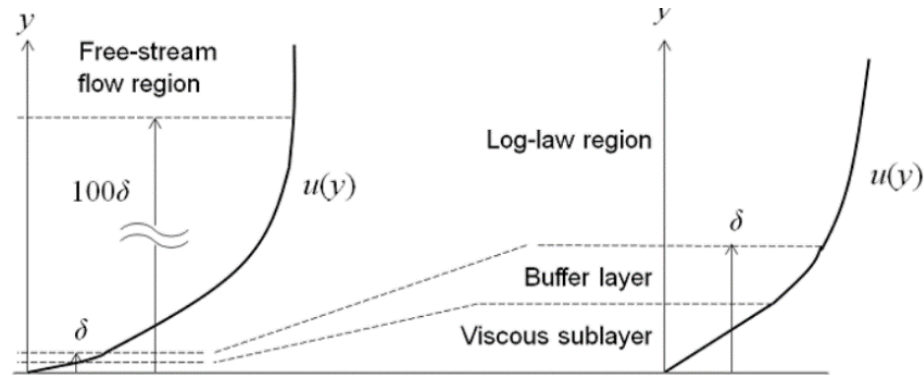


Figure 2.6. Near a solid boundary, a typical mean velocity profile. (Frei 2013)

- Laminar, viscous or linear sub-layer: Viscosity dominated region, the layer is very thin, closer to the wall, in which viscous forces prevail and velocity changes in linear fashion with distance from the wall, starting from 0 at the wall.
- Buffer layer: Turbulent dominated region where the flow starts to transform from transition to turbulent. Buffer layer is thicker than viscous sub-layer.
- Log-law layer: The mean velocity is proportional to the log of the distance to the wall in a fully turbulent region.
- Outer layer, or Free-stream flow region, or law-of-the-wake: Broad layer of turbulent region outside the buffer layer in which the gradient of mean velocity is zero.

In these layers before describing the flow conduct, the dimensionless distance to the wall and dimensionless velocity, y^+ and u^+ respectively must be defined:

$$u^* = \frac{U}{u_\tau} = f(y^+) \quad , \quad y^+ = \frac{\rho u_\tau y}{\mu} \quad 2.30$$

Where:

U = Mean Velocity

$$u_\tau = \text{Shear Velocity} = \sqrt{\tau_\omega / \rho}$$

$$\tau_\omega = \text{Shear stress at the wall} = \mu \frac{\partial U}{\partial y}$$

The viscous sub-layer, according to (Versteeg and Malalasekera 2007) is located at about $y^+ < 5$ which is in reality infinitesimally fine. When the boundary condition is implemented, i.e., if $y = 0$ then $U = 0$ and integrating the shear stress with respect to y , the distance to the wall and the mean velocity linear relationship is achieved.

$$U = \frac{\tau_\omega y}{\mu} \quad 2.31$$

following a little algebra, $u^+ = y^+$. 2.32

A further relation among u^+ and y^+ is established there in log-law layer $30 < y^+ < 500$, according to (Versteeg & Malalasekera 2007):

$$u^+ = \frac{1}{K} \ln(Ey^+) \quad 2.33$$

Where:

E = additive constant ≈ 9.8 (for smooth walls)

K = von Karaman's constant ≈ 0.4

In all four of these regimes, the flow field can be computed. The RANS and LES turbulence models, however, use wall functions to avoid using a quite fine mesh nearer to the wall, which basically relates the turbulent kinetic energy (TKE), mean velocity as well as the rate of dissipation to the local shear stress.

More information on turbulence can be found in (Schlichting 1979, White and Corfield 2006, Versteeg and Malalasekera 2007).

2.9 Computational Fluid Dynamics (CFD) modeling

2.9.1 Computational Fluid Dynamics (CFD) in industry

Computational Fluid Dynamics (CFD) is a sub-discipline of fluid mechanics, for solving mathematical models that can be used to demonstrate any type of fluid flow, for this it uses numerical algorithms and approaches. Said by (Versteeg and Malalasekera 2007) Computational Fluid Dynamics (CFD) is the study of processes incorporating transfer of heat, flow of fluids and related processes using computer-based simulations. The technique is extremely versatile and can be applied to both industrialized and non-industrialized environments. Few examples are as follows:

- Aircraft and vehicle aerodynamics: lift and drag.
- Ships' hydrodynamics
- Power plant: combustion in gas turbines as well as internal combustion engines.

- Turbomachinery: Diffusers, Flows inside rotating passages, as well as other similar devices
- Electronic and Electrical engineering: chilling of devices, such as microcircuits
- Chemical process engineering: polymer moulding, separation, and mixing.
- Buildings' internal and external environments: heating/ventilation and wind loading.
- Marine engineering: loads on offshore structures.
- Oceanography and hydrology: oceans, estuaries, and flows in rivers.
- Hydraulics: weirs, locks, flow in channels as well as other hydraulic structures.
- Meteorology: forecast of weather.
- Biomedical engineering: flow of blood via veins and arteries.

(Versteeg and Malalasekera 2007) says that Computational Fluid Dynamics (CFD) has been utilized in industrial applications since the 1990s, due to the fact that CFD has very user-friendly environment, it has low cost that in return sparked renewed interest in CFD.

The numerical algorithms that can solve fluid flow challenges are structured into CFD codes. Both commercial CFD packages offer user-friendly environment for entering problematic factors and examining the outcomes to make available simple entry to their resolving capacity. Therefore, every code has three essential components: 1) a pre-processor, 2) a solver, and 3) a post-processor.

It is worth noting that fundamental physics is quite convoluted when it comes to solving problems involving fluid flow, and the outputs provided by Computational Fluid Dynamics (CFD) codes are only as good as the physics or chemistry encoded in them at best and only as good as its user at the very worst.

It is difficult to evaluate the authenticity of the physics and chemistry models encoded in a programme as complicated as a Computational Fluid Dynamics (CFD) codes, or the precision of its end outcomes, without comparing them to experimental test results.

Anyone serious about using Computational Fluid Dynamics (CFD) must understand that it is not a replacement for experiment investigation, Instead, it's a very effective additional problem-solving tool that's key for minimizing design budgets.

2.9.2 Computational Fluid Dynamics (CFD) in confluences

Nevertheless, a CFD model of a confluence has the potential to perform well, applying it to realistic far reaches challenges or networks of open channel is expensive and, in several situations, impossible. In this case rather a 2D model may be used, in which the equations that governs the motion of fluid are applied in two dimensions and the variable in depth wise are averaged, resulting in the commonly recognized two-dimensional depth-averaged shallow water equations.

(Dinh Thanh, Kimura et al. 2010) used the experimental findings of (Weber, Schumate et al. 2001) for the validation of four variant of 2D depth-averaged shallow water models in a 90° open-channel confluence with and without the secondary current impacts. The models with secondary current effect capture the most distinctive features, clearly indicates a high level of potential application to a real-world open-channel junction flow. Because it can't replicate vertical mixtures or three-dimensional currents, by itself, it can only be a rough approximation for many other challenges, like sediment transportation (which they have not studied).

In three dimensions several numerical model analyses of junctions were carried out and published, each of which evaluated distinctive modelling methods and yielded some noteworthy conclusions. (Huang, Weber et al. 2002) and (Dordevic 2012) used physical model findings from (Weber, Schumate et al. 2001) to validate computational models in a 90° sharp-edged open-channel junction.

(Lira 2014) other recent research focused on the sharp-edge open-channel junction. Used the same CFD model (OpenFOAM) as in the similar research, but with a "rigid lid" approach and yielded some remarkable outcomes. However, the main drawback of this method is that it does not allow us to catch free surface.

There is possibly no other study in the literature that offers as comprehensive a collection of findings from physical model studies of confluences as (Weber, Schumate et al. 2001). According to these publishers, preceding research articles findings are restricted to 1D or 2D velocities and is more often reliant on dye trace visualization for flow explanation. The collection of data represented consisted of a fine grid turbulence and three-dimensional velocity computations for six orders of flow including mapping of water surfaces for four of these six orders of flow that laid down a standard for a 3D CFD model verification.

The figures below depict the numerous forms of experimental results that were given: Figure 2.7a illustrates the nondimensional longitudinal (lengthwise) velocity (u^*) projections, while Figure 2.7b presents the cross-sectional velocity projection, (nondimensionalized by the mean velocity at exit i.e., $U_t = 0.628$ m/s), Figure 2.8 presents the velocity components vertical profiles, Figure 2.9 depicts the vectors of velocity at section $x = -2$, Figure 2.10 displays the mapping of water-surface, and Figure 2.11 illustrates the turbulent kinetic energy (k). Though seven separate scenarios were investigated, All the illustrations are associated to single flow condition (discharge ratio), and in this scenario equates to 0.25, defined as:

$$q^* = Q_m / Q_t \quad 2.34$$

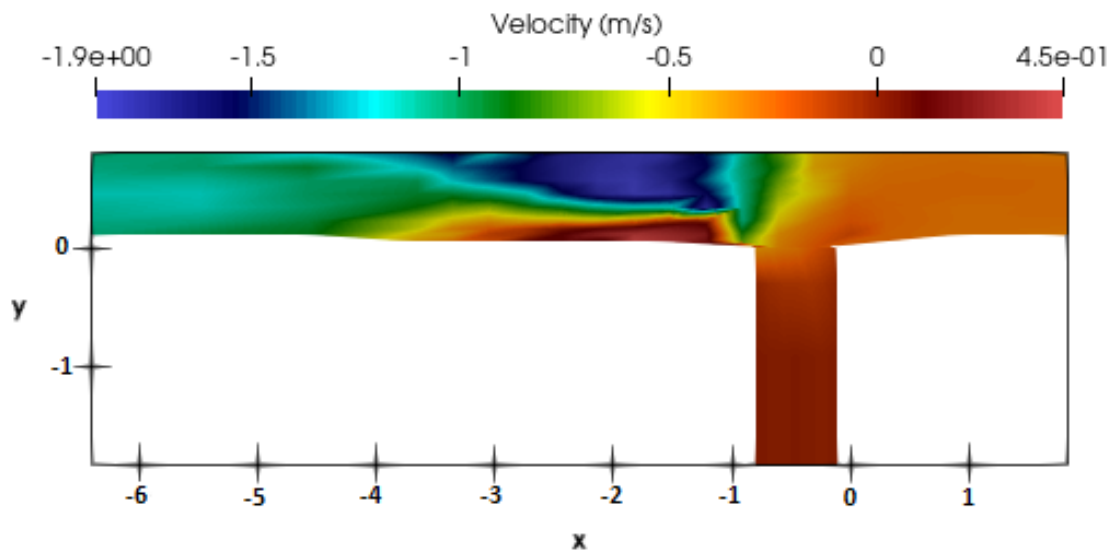
Where:

q^* = Discharge ratio

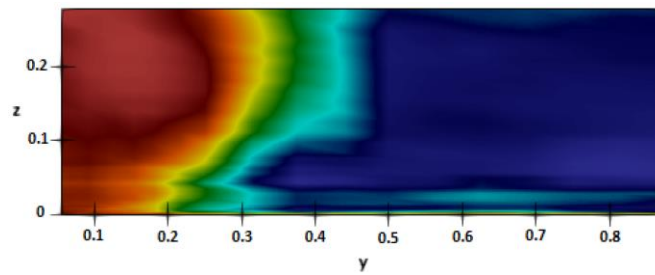
Q_m = Main Channel Discharge

Q_t = Total Discharge.

To render the coordinates nondimensional, they were divided by the channel width (W), which is 0.914 meters. (Weber, Schumate et al. 2001) provided the following experimental findings.



(a)



(b)

Figure 2.7. (a) Plan view Dimensional longitudinal (lengthwise) velocity (u^*) projections at ($z/W = 0.278$) and (b) cross-sectional velocity projection at ($x/W = -2$) (Weber, Schumate et al. 2001)

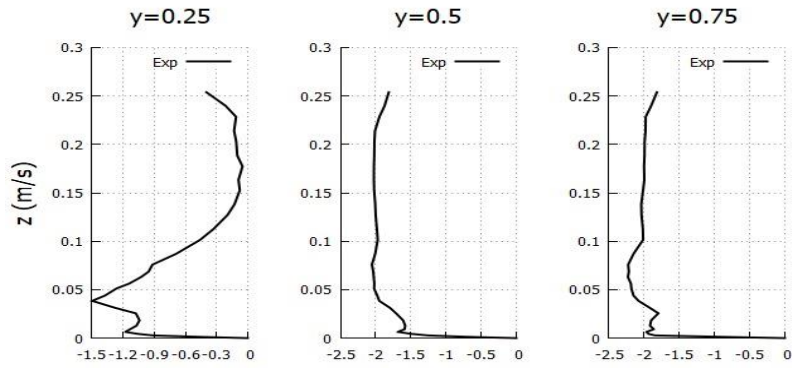


Figure 2.8. Exp. Streamwise Velocities at $x/W = -2$ (Weber, Schumate et al. 2001)

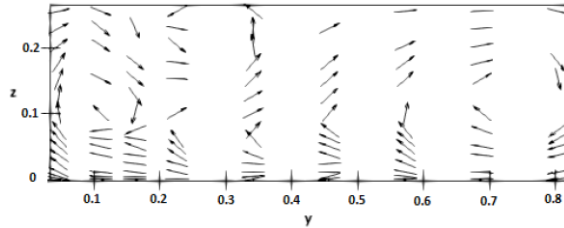


Figure 2.9. Velocity vectors at Cross-section ($x = -2$) (Weber, Schumate et al. 2001)

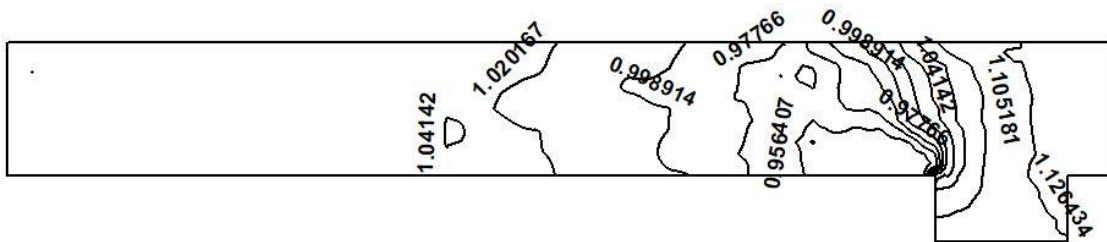


Figure 2.10. Exp. Water-surface mapping (Weber, Schumate et al. 2001)

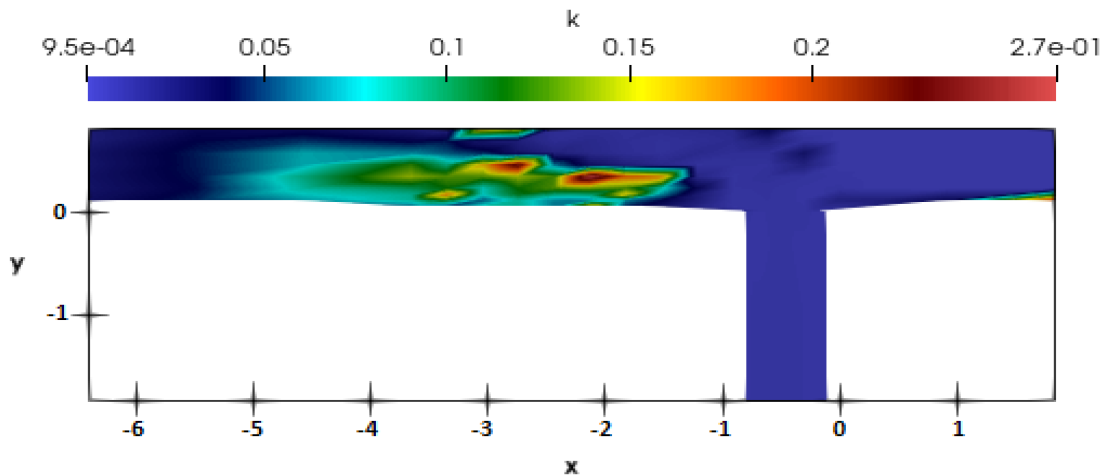


Figure 2.11. Distribution of TKE ($z/W = 0.278$) (Weber, Schumate et al. 2001)

From these and the other projections for various flow scenarios and from various regions can be used to create a comprehensive explanation of the flow arrangement in the immediate area of a junction. Flow patterns have the following key features:

- Just downstream of the intersection in the left wall, the separation region (dark red region represented in Figure 2.7) forms. It consists of a recirculation region in the center with upstream movement of the positive velocities and an outermost portion with extremely low velocities that differentiates the streamwise flow from the recirculation region.
- At section $x = -2$ just downstream of the intersection in the principal channel on the right-side bluish region can be seen as depicted in Figure 2.7, represents maximum longitudinal velocities (u^*) that has been constricted by the separation zone.
- The separation area expands and elongates as discharge ratio (q^*) reduces, i.e., since very little discharge enters the primary channel enabling the primary channel to constrict furthermore, leading to increased velocities in the contractual region. When sufficient flow enters from the side channel, the lateral

flow's reflection off the opposite wall begins to collapse the separation zone downstream end, adequately narrowing the region. This pattern goes past a certain point. Within these experimental tests, only discharge ratio (q^*) = 0.083 exhibited this characteristic, among the seven scenarios, only discharge ratio (q^*) = 0.25 represents the widest zone of separation.

- The free surface flow projections and the projections at the channel's base do not match; the zone of separation close to the free surface is broader and longer with more recirculation within it.
- Around the channel intersection upstream edge there is a stagnation point represented by very low velocities, though it is not properly depicted in the former figures.
- As shown in Figure 2.8, Along the downstream channel, a clockwise helicoidal current is formed. These helicoidal currents are formed by the impact of branch channel flow against the wall opposite of the intersection due to which the flow is reflected downwards as at the surface has greater velocities, and downstream (d/s) by the oncoming water in the main channel. On the way back, the flow is deflected upward into the zone of separation when it approaches the bottom of the channel and meets the left side bank downstream channel. The whole channel is eventually surrounded in a massive clockwise secondary current, which diminishes as it travels downstream.
- Figure 2.10 depicts the mapping of the water surface. Water surface profiles usually show a drawdown as the flow enters the constricted area, followed by a depth rise downstream of the channel as the flow reaches the maximum channel width for all flow scenarios. In the major channel the maximum depth at upstream is $1.104H_0$, whereas H_0 is the average depth at downstream, 31mm more than the average depth while lowest water depth is found in the constricted region i.e., $0.916H_0$, 25mm less than the average depth, for flow condition $q^* = 0.25$.

Relying on the knowledge above, the sensitive area to be modelled is between $x = -1$ and -4 in the downstream channel, where the flow is more turbulent, intense, and three-dimensional, necessitating the validation of any Computational Fluid Dynamic (CFD) model.

By taking into consideration these experimental observations, (Huang, Weber et al. 2002) created a confluence and justified a Computational Fluid Dynamics (CFD) model that discretizes the governing equations using the Finite-Volume Method (FVM). Used standard k-Epsilon ($k-\epsilon$) model for closure and mesh regeneration technique was used which enables the grid to be molded as per the computed surface of water throughout the iterations until get to convergence. Instead of using the cumbersome Volume of Fluids (VOF) technique, that deals with multiphase flow (water and air), this technique is capable of capturing the conduct of free surface water. The influence of the flow behavior on the intersection angle was also investigated in the study.

(Dordevic 2012) examined three case studies; 1) Data obtained by the author at the Danube River (in Belgrade), 2) Confluence at a 30° angle by (Biron, Best et al. 1996), and 3) Experimental findings by (Weber, Schumate et al. 2001), with the growing complication of the confluence morphology. The closure was performed by using standard k-Epsilon ($k-\epsilon$) turbulence model but considering the free-surface as a Rigid lid (RL), that assumes the surface to be static and non-frictional, using the software Sediment Simulation in Intakes with Multiblock (SSIIM2), which uses the finite-volume method (FVM) as well.

(Dordevic 2012) based his research on the assessment of experimental and computed velocity profiles. Only one flow ratio scenario, $q^* = 0.583$, was examined in this case.

(Ramamurthy, Han et al. 2013) provided an important study that, while not directly about confluences, was extremely helpful in the job presented here. They developed a model that was extremely three-dimensional (3D) for a channel bend flow, due to the mutual influences of the flow separation and secondary flows along its internal bend

wall, both of which are features seen in the confluences. For the calculations, the softwares Fluent and Phoenix were used. Four water surface treatments, including Volume of Fluids (VOF) methodology, Height of Liquids (HOL), Porosity principle (POR), and Rigid Lid assumption (RL), and three turbulence models, including Large Eddy Simulation (LES), Reynolds stress Model (RSM), and RNG k-Epsilon ($k-\epsilon$) model, were used to compare experimental results with secondary flows and flow separation.

(Lira 2014) contributed a significant piece of work that was specifically related to confluences and was highly helpful in the work performed here. In this study, three turbulence models ($k-\omega$, RNG $k-\epsilon$ and LES) were used. “Rigid Lid” assumption was used for the treatment of free surface. The programme he used in his research was OpenFOAM. Comparison of vertical profiles of streamwise velocities with experimental results using three different turbulence models by (Lira 2014) are depicted in Figure 2.12 to 2.17.

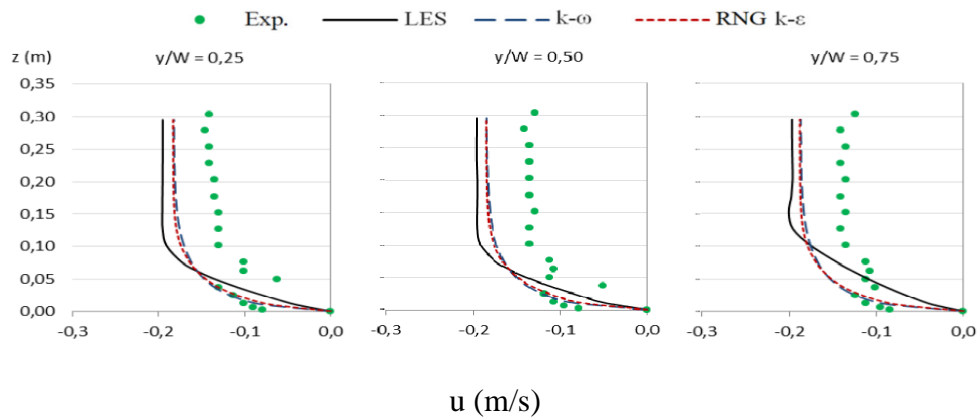


Figure 2.12. Profiles of vertical streamwise velocities at $x/W = 1$ from (Lira 2014)

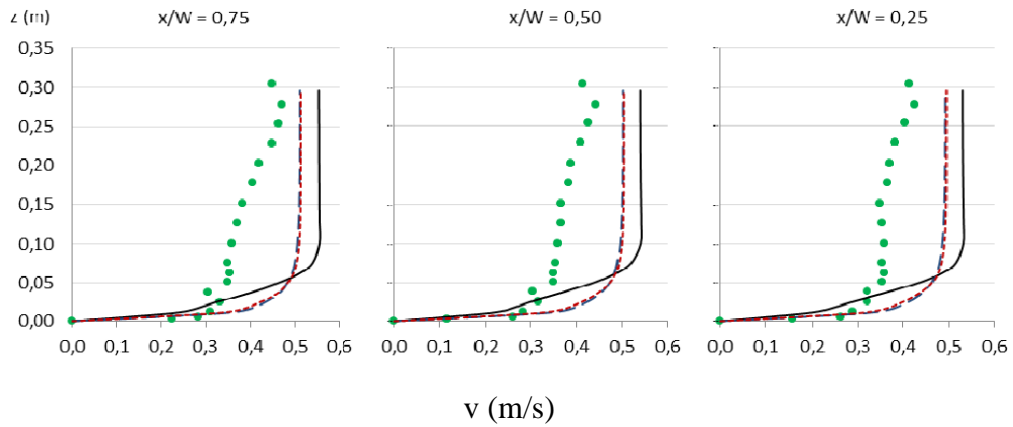


Figure 2.13. Profiles of vertical streamwise velocities at $y/W = -1$ from (Lira 2014)

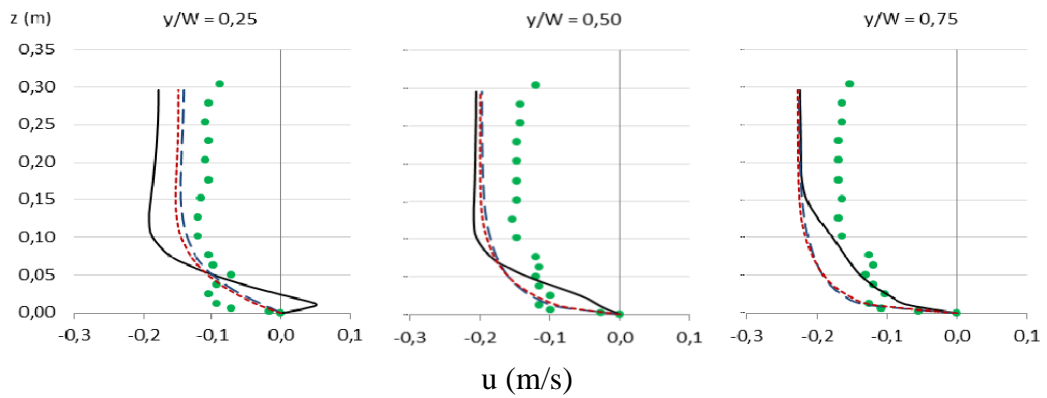


Figure 2.14. Profiles of vertical streamwise velocities at $x/W = 0$ from (Lira 2014)

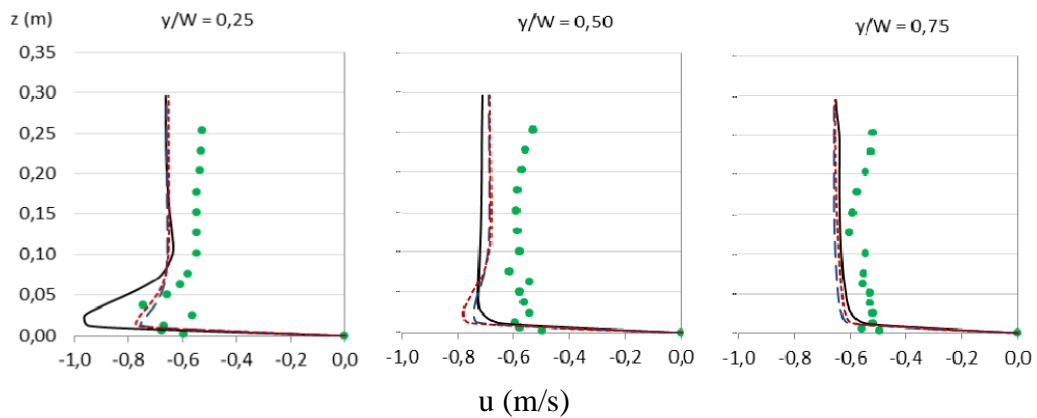


Figure 2.15. Profiles of vertical streamwise velocities at $x/W = -1$ from (Lira 2014)

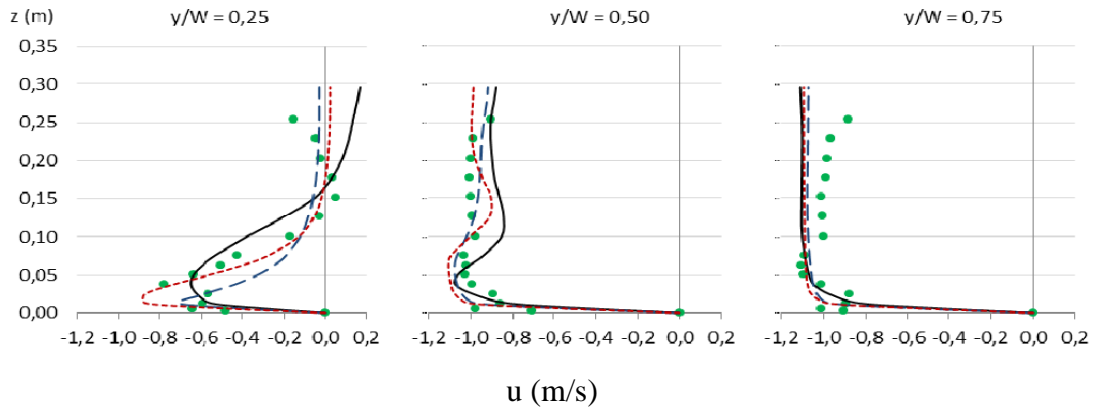


Figure 2.16. Profiles of vertical streamwise velocities at $x/W = -2$ from (Lira 2014)

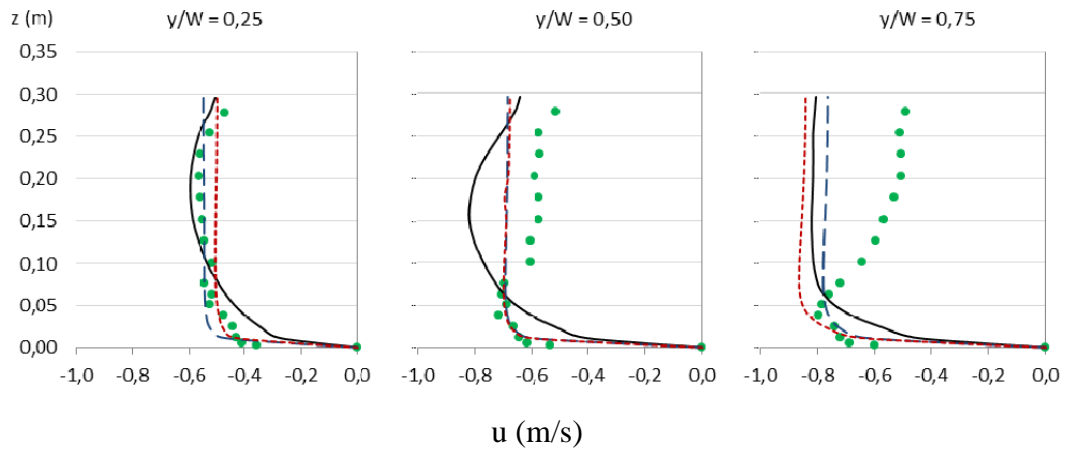


Figure 2.17. Profiles of vertical streamwise velocities at $x/W = -6$ from (Lira 2014)

There is compelling agreement with the experimental outcomes in the above comparison of vertical profiles of streamwise velocity made by (Lira 2014), but all the calculated results using three different turbulence models are slightly higher than the experimental results.

Based on previous research into the simulation of a 90o open-channel junction flow, it is thought that evaluating OpenFOAM (CFD) software, which is free and open-source, using different modelling techniques than those previously tested in the literature, and validating them with (Weber, Schumate et al. 2001) experimental results, would be valuable.

2.9.3 Open Field Operations and Manipulation (OpenFOAM)

OpenFOAM is a completely freely available CFD toolbox software package. As per OpenFOAM (2014), the software has a huge number of users in certain disciplines of engineering and science both from academic and industrial agencies. Which has a wide variety of applications that can be used to overcome problems ranging from complicated flow of fluids including heat transfer, chemical reactions and turbulence to electromagnetics and solid dynamics. The Finite Volume Method is used in its solvers.

One of the most appealing features of OpenFOAM is that it has no purchase price, allowing smaller businesses, individuals, and academic staff to benefit from such a powerful software package without having to pay for CFD software or a yearly license. It contains a decent post-processor called ParaView, but the key drawback of it is that, like all commercial CFD packages, it lacks a user interface that will allow the operator to pre-process the model easily and quickly.

OpenFOAM was designed to run exclusively on Linux, which can be challenging for those unfamiliar with the operating system. Figure 2.18 shows how an OpenFOAM case's basic directory is organized.

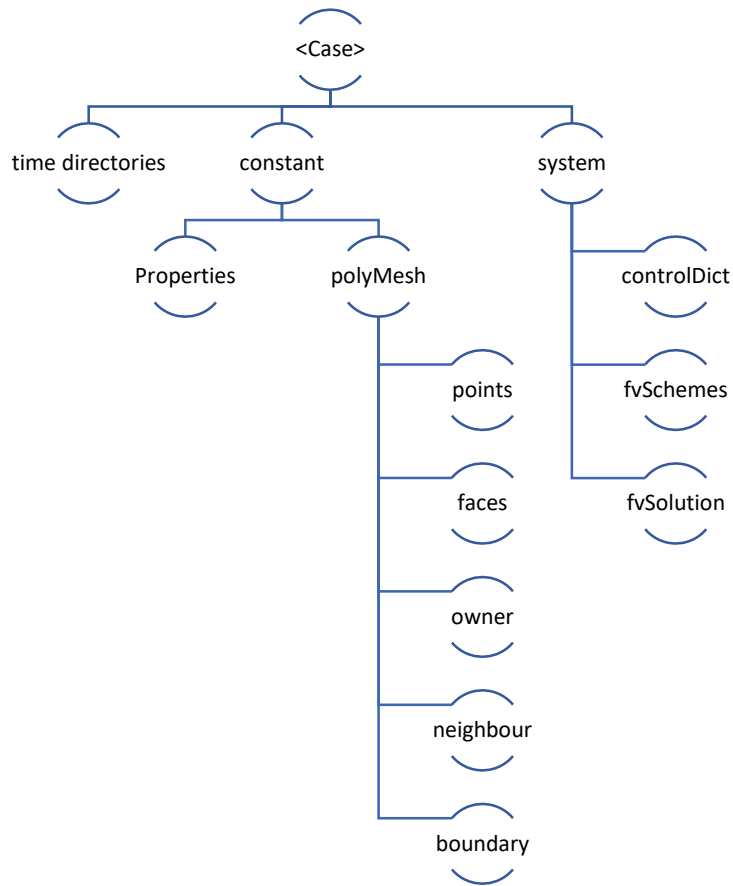


Figure 2.18. Structure of the OpenFOAM case directory (OpenFOAM 2014)

To every modeling scenario, the developer must build a folders directory in this operating system to standardize the files. Mesh and Domain must be rewritten in the system folder's blockMeshDict file, which generates other geometry files (points, faces, etc.) in the polyMesh constant subfolder after running the blockMesh command. The turbulence model you choose is broken down into files in the Properties folder. The initial and boundary requirements are defined into time folders in files inside the subfolder 0 since the case is assigned to begin at time $t = 0$. The controlDict file in the system directory is used to specify control parameters. The numerical schemes are listed in the system directory files fvSchemes and fvSolution. When the case is executed, the

modeling outcomes will be created automatically and are stored in the time directory inside the 0 subfolder, depending upon the time steps defined in the controlDict file.

The advantage of being unable to push buttons as in commercial software is that the individual is required to dive further into numerical methods and modelling features, potentially qualifying her or him as a thoughtful and responsible consumer.

Also, in the most complex cases, OpenFOAM has been commonly used in hydraulic simulations. Unfortunately, very limited OpenFOAM models of open-channel flows, and perhaps nothing on confluence modelling, have been researched in literature.

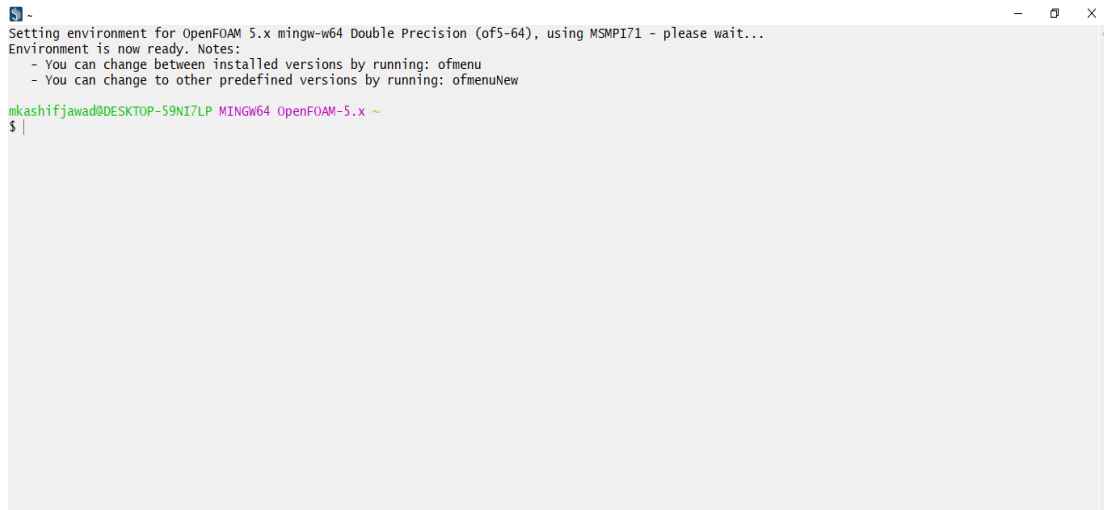
All of these factors make it difficult for new OpenFOAM users, especially those who are just getting started with open channel modelling, to succeed in a steep but hopefully rewarding learning curve.

METHODOLOGY

3.1 The 3D Open-Source Model OpenFOAM

OpenFOAM, an open-source and freely accessible CFD software also recognized as Open Field Operation and Manipulation, has been used to perform the simulations. It is a software based on the Linux operating system written in the language of C++. OpenFOAM also has a version that can be installed and run on a Windows operating system. Since OpenFOAM is an open-source programme, its features can be modified and adapted to meet specific needs.

Initially, the OpenFOAM framework, the resources available and also how to implement them appropriately took a little time.



```
Setting environment for OpenFOAM 5.x mingw-w64 Double Precision (of5-64), using MSMPI71 - please wait...
Environment is now ready. Notes:
- You can change between installed versions by running: ofmenu
- You can change to other predefined versions by running: ofmenuNew
mkashifjavad@DESKTOP-59NI7LP MINGW64 OpenFOAM-5.x ~
$ |
```

Figure 3.1. BlueCFD Terminal Interface

Deciding which solver to use was an important task. PisoFoam (transient solver to treat the surface as a rigid lid for an incompressible single fluid), this implies that by implementing a top boundary ("lid") without friction, the free-surface would be fixed at

a certain depth, the same approach used for example, by (Dordevic 2012). The interFoam solver (for two incompressible, isothermal immiscible fluids employing a Volume of Fluid (VOF) method) was then utilized to examine the water-surface variation. The $k-\omega$ SST model was used as the turbulence model in this parametric analysis.

3.2 Volume of Fluid Method (VOF)

One of the issues with NS-Equation is that it cannot numerically capture moving free surfaces. The Volume of Fluid method can deal with complex free surfaces, but its application is limited due to the high computational cost (Ai, Ding et al. 2017). To model and research wave induce forces, the VOF method is commonly used in the NS- equation (Vu, Ahn et al. 2016).

3.3 Solution Domain

The domain lengths and widths used in the numerical model were identical to those used in the flume constructed by (Weber, Schumate et al. 2001) in the experiment, the solution domain is portrayed in 2D in Figure 3.2. Water flows into the domain from both inlets, 0.0425 m³/s from the main inlet and 0.1275 m³/s from the branch channel, and out the outlet. There are two inlet patches, one outlet patch, an atmosphere at the top, and three different types of walls: right wall, left wall, and bottom wall.

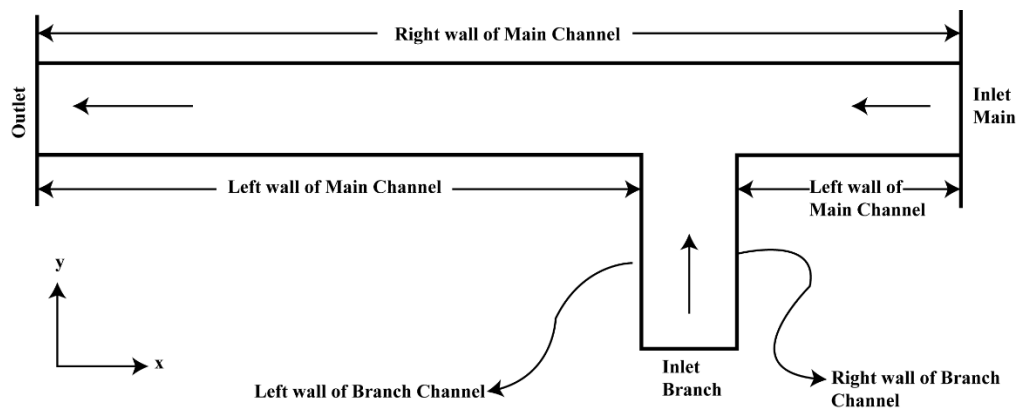


Figure 3.2. 2D Representation of Domain

3.4 Geometry

The simulation domain is defined by mesh and geometry. The fundamental prerequisite for a numerical simulation in OpenFOAM is domain geometry and meshing. One of the three methods for generating mesh for OpenFOAM can be used. Either by using the OpenFOAM tools blockMesh and snappyhexMesh, or by using a third-party tool such as Gmsh, Salome, or fluentMesh. OpenFOAM can easily convert meshes created by third-party software.

It is necessary to establish that grid independent outcomes have been achieved from the grid. In particular, close to the wall boundaries and the junction, which is the region of rapid variation, the grid structure must be fine enough. The geometry is divided into 15 blocks to accomplish this. The cells in the z-axis were kept constant, 27 cells, while the cells in the x-direction and y-direction varied to refine the geometry's area of interest, the junction region. The smallest dx was 0.013m, while the smallest dy was 0.017m. Various computational flow experiments were conducted with various numbers of grids. The refined mesh with 827904 cells was used as a final mesh, created by using blockMeshDict, here is a view of our coarser mesh as shown in Figure 3.3.



Figure 3.3. Plan view of coarser mesh

It can be seen from the figure that junction region is finer than that of upstream and downstream of the channel. This decision could be explained by the fact that streamwise velocity gradients are not large in these regions and that a fine grid is therefore not

required. Higher refinement, on the other hand, was achieved in the separation zone region.

3.5 Boundary Conditions

Atmosphere, Outlet, walls and Inlets are the four separate boundary types exists in the domain. The (Guide 2020) or (Foam 2017) literatures include a comprehensive description of the boundary forms and their meanings.

For the scenario's ultimate output [(variableHeightFlowRateInletVelocity) (Mixed BC)] has been used by specifying a defined flow rate of 0.0425m³/s and 0.1275m³/s at the main and branch channel inlets respectively, allowing for free water level fluctuation [(variableHeightFlowRate (Mixed BC))], as well as maintaining a continuous average velocity at the outlet by defining an (inletOutlet) BC.

FixedFluxPressure was designated on the pressure boundary conditions on the walls as well as on inlets, that controls the pressure distribution so that the velocity boundary condition determines the flux on the boundaries (Neumann BC). (inletOutlet) BC was implemented at the Outlet.

The topmost surface of the grid was treated as a free surface since they were exposed to ambient pressure which could permit flow to readily get in and out of the domain and was accomplished by employing a velocity (pressureInletOutletVelocity) BC that belongs to Mixed BC as an outflow condition and specifying the total pressure value [totalPressure] from Dirichlet boundary condition.

In relation to Boundary conditions of Turbulent kinetic energy (k), Omega (ω) and Turbulent kinematic viscosity (ν_t) in walls, they demand special attention due to the fact that viscous flow area connected to solid bodies (Bayon, Valero et al. 2016). In the case of k, kqRWallFunction has been used, that actually serves as a Neumann BC, for ω , omegaWallFunction has been used, that offers a condition for cases of turbulent flow with a high Reynolds number (Foam 2017), in case of ν_t , nutkWallFunction has been

used, centered on turbulent kinetic energy offers a turbulent kinematic viscosity condition (Foam 2017).

3.6 Modeling with OpenFOAM

The pre-processing work outlined in this chapter constituted of building a best possible geometry and defining suitable boundary conditions, and lastly selecting the appropriate parameters of control. Although many intermediate scenarios have actually happened, only the final settings are discussed in detail.

There are three key steps to modelling in OpenFOAM.

- Preprocessing
- Processing
- Postprocessing

3.6.1 Preprocessing

Preprocessing is the most critical phase in a numerical simulation since it decides whether the simulation will finish, and the results will be useful. The model reads these files during the simulation and prepares all the appropriate files for the numerical simulation. Inside the case folder, there are three directories for preprocessing files. The folders are.

- 0 folder (initial conditions)
- Constant (Physical properties)
- System (settings for simulation)

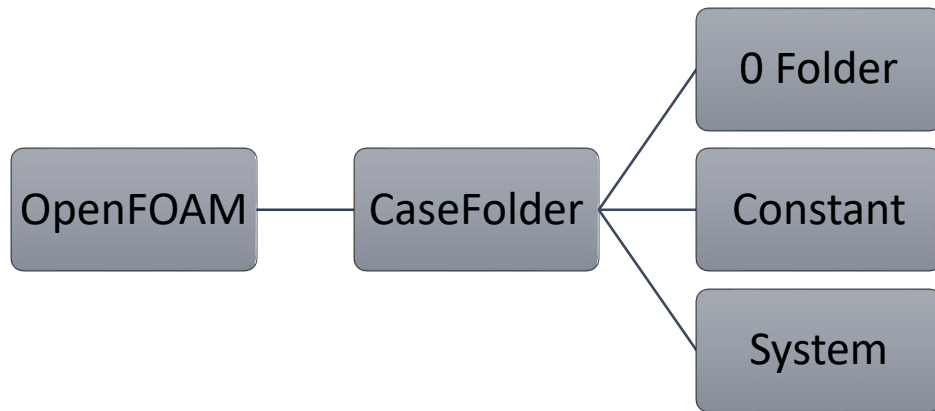


Figure 3.4. Basic Structure for OpenFOAM Directories

3.6.2 0 Folder (Initial Field Values)

The boundary conditions and initial field values must be specified in OpenFOAM. These values and boundary conditions are described in directories in 0 folders, which correspond to the values at time 0.

At the patches and walls, these values enforce boundary conditions. There are six directories for this particular case:

- U (velocity)
- k (turbulent kinetic energy)
- p_rgh (pressure divided by density)
- alpha.water (Phase fraction)
- Nut (Turbulent viscosity)
- Omega (Specific energy dissipation rate)

The discharge ratio (q^*) equals 0.25 was selected to be analyzed in this study. In terms of three-dimensional flow patterns, this is the most severe case, and thus the most difficult scenario to replicate in modeling. The flows at the inlets therefore had to be set to $0.0425 \text{ m}^3/\text{s}$ (Q_m) and $0.1275 \text{ m}^3/\text{s}$ (Q_b) respectively for the primary and secondary

channels. To put that into practice, following set of boundary conditions were used as shown in table below.

Table 3.1 Summary of Initial conditions

	Inlet	Outlet	Walls	Atmosphere
Velocity	variableHeightFlowRate InletVelocity	inletOutlet	fixedValue	pressureInlet OutletVelocity
alpha.water	variableHeightFlowRate	inletOutlet	zeroGradient	InletOutlet
Omega	fixedValue	inletOutlet	omegaWallFunction	zeroGradient
p_rgh	fixedFluxPressure	inletOutlet	fixedFluxPressure	totalPressure
Nut	zeroGradient	inletOutlet	nutkRoughWallFunction	Calculated
K	fixedValue	inletOutlet	kqRWallFunction	zeroGradient

Boundary conditions are explained in section 3.5.

3.6.3 Constant Directory

This directory remains the same in the solution, as the name implies. This directory defines the physical properties of the two phases, which are:

Table 3.2 Physical properties of Water and Air

Phases	Density (Kg//m³)	Kinematic Viscosity 10⁻⁵
Water	1000	0.5
Air	1	1.48e ⁻⁰⁵

The three subdirectories are:

- G (Gravitational acceleration)
- Transport Properties
- Turbulence Properties

3.5.4.1 Transport Properties

The transport properties of the two phases are described in this directory. Both phases are Newtonian fluids, which means that viscous stresses caused by flow are proportional to strain, or the rate of change of deformation in the fluid. The dynamic viscosity of both fluids is also described in this directory using the relationship between kinematic viscosity and Reynolds number.

$$R_E = \frac{R_h V}{\nu} \quad 3.1$$

The Reynolds number is Re , the hydraulic radius is R_h , the mean velocity is V , and the kinematic viscosity is ν . The density of both fluids is also defined, with 1000kgm^{-3} for phase 1 and 1kgm^{-3} for phase 2.

3.5.4.2 Turbulence Properties

There are four different turbulent models for turbulent flows. One of the four models must be used for each simulation. Each one must be described separately for each simulation in this directory.

3.5.4.3 Gravitational Acceleration

G is the gravitational acceleration, which has a constant value of 9.98ms^{-2} and is represented in the negative Y direction in this directory.

3.6.4 System Directory

The settings that govern the simulation are contained in this folder.

3.5.5.1 ControlDict

The control settings to execute the case in OpenFOAM are generated in a file named `controlDict`. The solver used in the simulation is the first word in this dictionary. Since this is a case of multiphase flows, `InterFoam` was chosen as the solver. The following seven terms are for time control, which includes the initial time at which the simulation must begin. The `endTime` specifies when the simulation must be completed. `DeltaT` is

the time step, and writeControl and adjustableruntime indicate that deltaT must adapt to the simulation. The time interval at which the simulation results must be written is described by WriteControl. Writeformat and writePrecision, respectively, regulate the format and precision with which the results must be written.

The Implicit scheme was used to discretize the schemes. As a result, ensuring numerical stability and temporal accuracy was unnecessary, besides this a Courant number less than one was adopted. For one cell the Courant number (Co) is determined by using the preceding formula:

$$Co = \frac{\delta t |U|}{\delta x} \quad 3.2$$

Where:

δx = Size of a cell in velocity direction

$|U|$ = the velocity magnitude of this cell

δt = the time step

3.5.5.2 DecomposeParDict

The quality of a simulation's result is almost always determined by the mesh quality, but the time it takes to simulate with finer meshes is a concern. As a result, it becomes necessary to achieve the computer's capabilities. A simulation can be performed in parallel in OpenFOAM. In decomposeParDict, the settings for running in parallel are specified. This dictionary describes the number of virtual cores used in a simulation.

3.5.5.3 SetFieldsDict

The setFieldsDict directory is used to set the initial field values for phases in the domain. The initial fields for the cells in which alpha.water must be specified are defined in this directory. This directory is used, for example, if initial field values for phase 1 must be specified up to a certain depth in the domain.

3.5.5.4 FvSchemes (Finite Volume Schemes)

From a list of choices offered by OpenFOAM, you can choose from a variety of numerical discretization schemes. These are not explored in depth in this analysis. The numerical schemes that have been adopted are presented in Table 3-3.

Table 3.3 Numerical schemes adopted.

Type	OpenFOAM keyword	Chosen Scheme
Flux calculation	fluxRequired	None
Surface normal gradient scheme	snGradSchemes	Corrected
Time scheme	timeScheme	Euler
Divergence scheme	divSchemes	Gauss limited linear
Laplacian schemes	laplacianSchemes	Gauss linear corrected
Gradient scheme	gradSchemes	Gauss linear

3.6.5 Processing

3.6.5.1 InterFOAM

The InterFOAM solver is used to solve two types of fluids: immiscible and incompressible. It is one of the OpenFOAM solvers that can capture interfaces between the fluid. InterFOAM is used in this case since this case simulates two phases, namely water and air.

3.6.5.2 PIMPLEFOAM

PIMPLE (Pressure Implicit Momentum with Pressure Linked Equations) is a hybrid algorithm that combines SIMPLE (Semi-Implicit Method for Pressure Linked Equations) as well as PISO (Pressure Implicit with Splitting of Operator). It is a predictor-corrector method.

3.6.5.3 Parallel Simulation

Simulations can be run on a single core or in parallel on multiple cores with OpenFOAM. The first step is to decompose the case and spread it through several cores using the `decomposePar` command. This command tells OpenFOAM to read the `decomposeParDict` file in the case directory's system folder, which is decomposing the case and distributing it to various cores. The benefit of running the simulation in parallel is that it makes full use of the computer's capabilities, allowing it to complete the process in much less time than if it were performed on a single core.

3.6.6 Post Processing

In a simulation, postprocessing refers to the processing of the outcome files and their proper shaping in accordance with the result requirements. In general, simulation results are almost unprocessed and useless unless they are properly processed.

The output of OpenFOAM is usually in the form of text files, with each cell for each parameter being read at each time stage. Hundreds of thousands of readings are present. It is impossible to read each and every one of the readings. As a result, the data must be post-processed with appropriate software.

3.6.6.1 ParaView

A package called ParaView is included with OpenFOAM, and it can read OpenFOAM files and generate views in the form of pictures and graphs.

ParaView is a powerful and user-friendly tool that can be used in a variety of fields, including structural analysis, climate science, astronomy, and computational fluid dynamics. ParaView has a number of functions for generating data visualization and rendering.

The findings are still in raw form, requiring more processing to satisfy the needs of the case.

The depth and velocity of the flow in a channel are important. If the depth reaches the channel's maximum depth, the surrounding areas are flooded, and if the flow rate is high, scouring and other problems occur. These two are interdependent, according to the

continuity equation. If the flow velocity is slow, the depth of the flow increases, and if the depth of the flow is less with the same amount of fluid, the flow velocity increases. As a result, depth contours and velocity vectors are computed at precise locations to ensure that the experimental results are accurate. Different depth contours at specific locations are needed for each test.

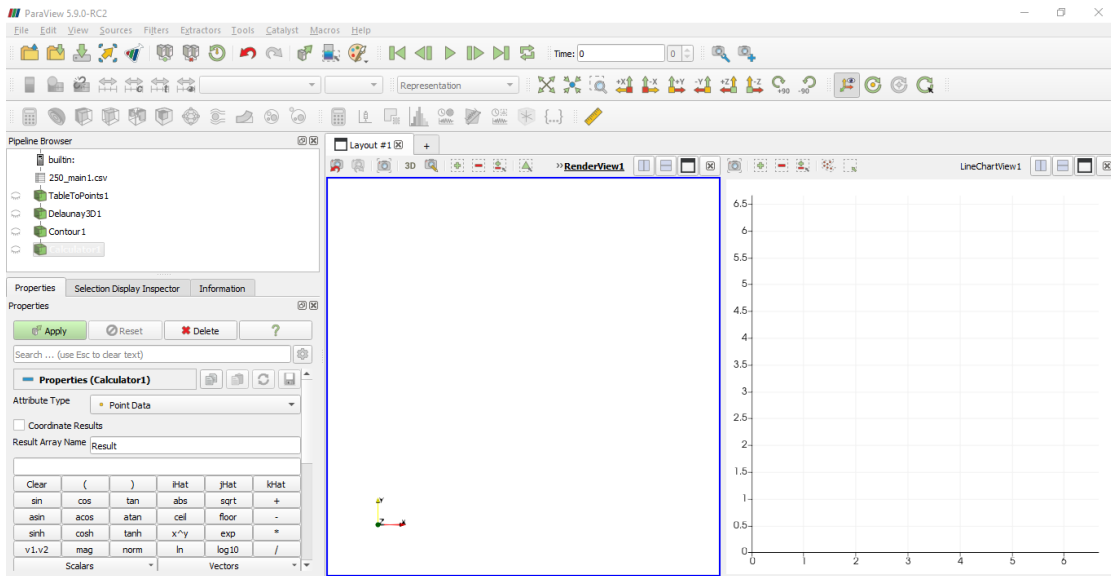


Figure 3.5. ParaView Interface

Other choices in Paraview include the development of.csv files for depth with the corresponding coordinates. This file can be imported into other software programmes such as CAD, ArcMap, and others to create line contours.

3.7 Study case

The experimental details of (Weber, Schumate et al. 2001)'s physical model analysis, utilized to validate the numerical model, are examined in this chapter. As seen in Figure 3.6, they investigated a sharp edged 90° open-channel junction in which the width of the channel was constant with smooth walls. On both the primary and secondary channels, head tanks provided the discharge. A honeycomb 100 mm thick and Perforated plates were installed at the primary and secondary channel inlets to guarantee a uniform

flow into the junction channels. The bottom steepness was zero. An adjustable tailgate in the channel downstream was used to monitor the depth of the tailwater.

As shown in Figure 3.6 and Figure 3.7, The coordinate system origin is positioned at the bottom of the channel intersection upstream edge. The channel breadth (W) equals 0.914 meters, or 3 feet was used to normalize all the distances. Mean velocity at the outlet (U_t) equals 0.628 m/s was used to nondimensionalize the velocity measurements. Q_t is the cumulative discharge at the tail of the channel, Q_m is the main channel discharge while Q_b represents the side channel discharge. Where cumulative discharge (Q_t) equals to 0.17 m³/s, and H_o represents the tail water depth which equals 0.296 meters. Both were maintained fixed that resulted in a subcritical flow with a mean velocity at the tail U_t equals 0.628 m/s and Froude number (F_r) of 0.37. From $q^* = 0.083$ to 0.917, seven different flow ratio scenarios were tested.

Although velocity was measured with an acoustic Doppler velocimeter (ADV) over a grid mentioned within the intersection region depth was measured with a point gauge. Using a time series of measured velocities from every position, the mean velocity and turbulence intensity were determined. Furthermore, a two-dimensional water surface mapping was conducted across the channel junction on a 72.2-millimeter square grid.

The locations of all velocity measures are depicted in (Figures 3.7-3.8). In the first figure, the cross-sections are shown and the vertical profiles locations in the second figure. In all, 15 to 17 more or less points for each vertical profile were recorded (positioned at elevations: 0.2 – 0.6 – 1.2 – 2.5 – 3.8 – 5.1 – 6.3 – 7.6 – 10.1 – 12.6 – 15.2 – 17.8 – 20.3 – 22.8 – 25.3 – 27.9 cm - and 30.4 cm, anywhere if required).

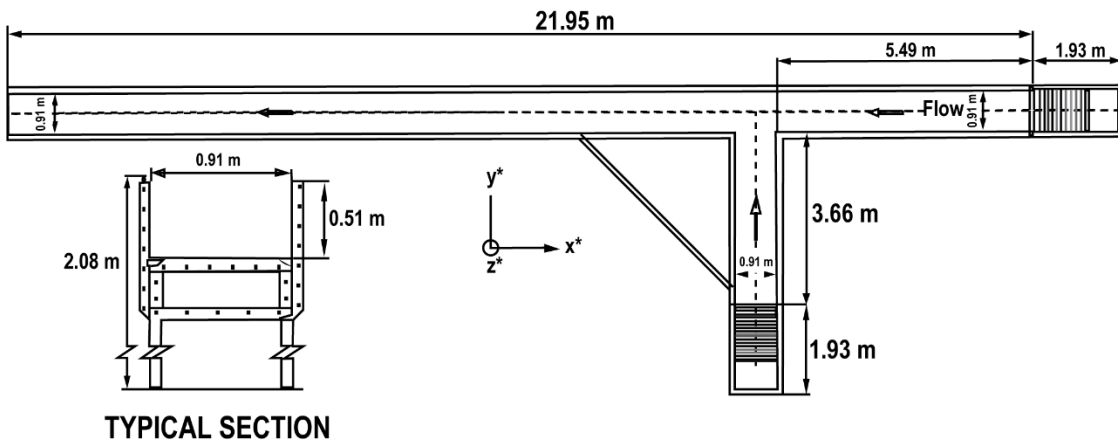


Figure 3.6. Laboratory Channel Layout (Weber, Schumate et al. 2001)

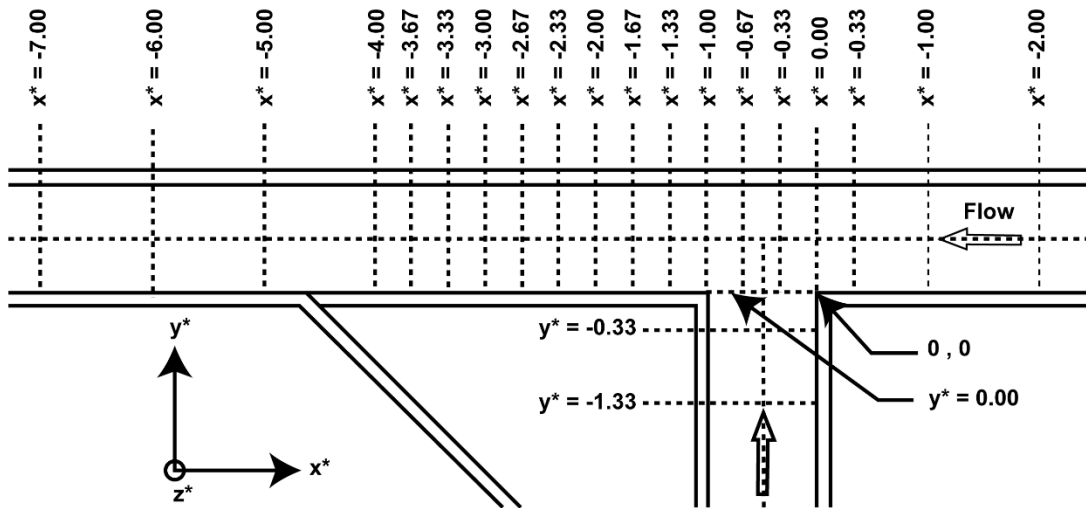


Figure 3.7. Position for gathering of data in a cross-section (Weber, Schumate et al. 2001)

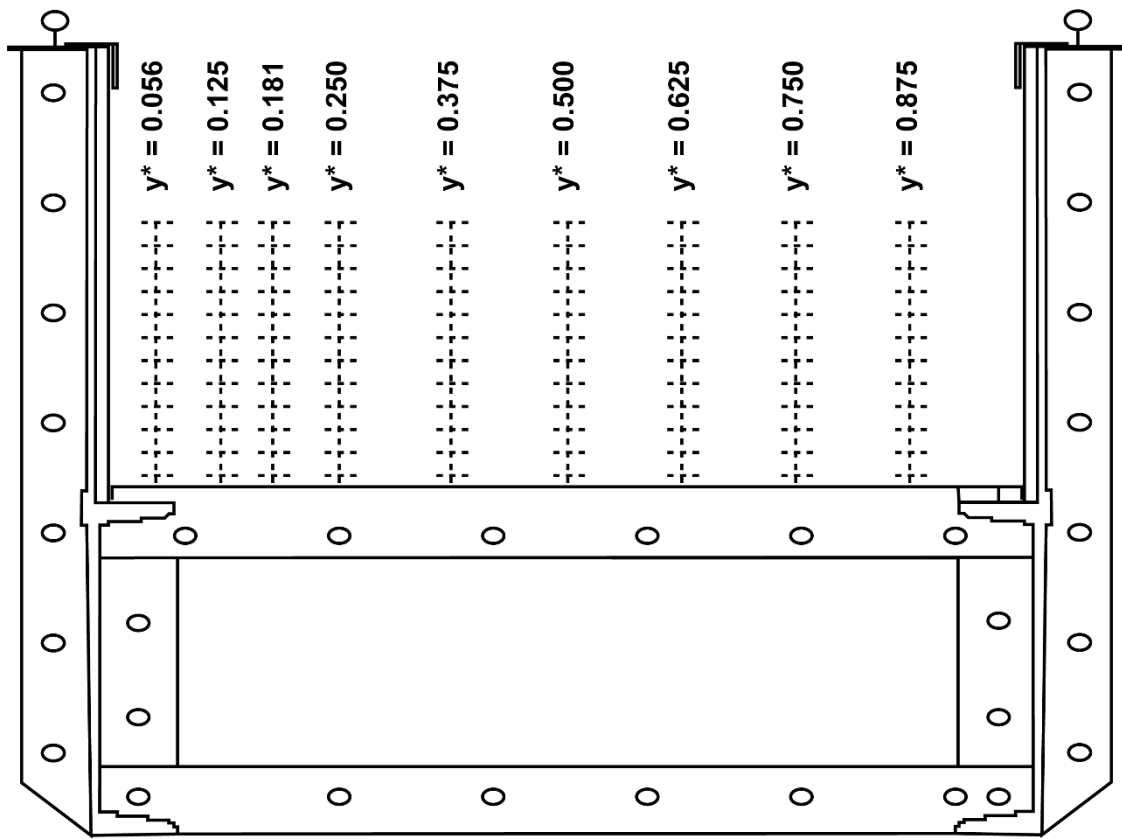


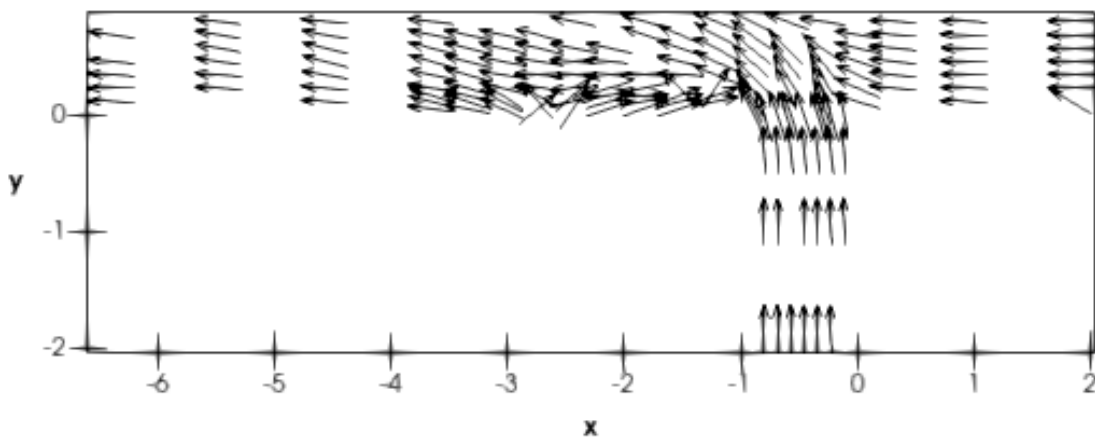
Figure 3.8. Stations for gathering of data for each cross-section (Weber, Schumate et al. 2001)

RESULTS AND DISCUSSION

4.1 Assessment of Velocity vectors in Plan view

To start examining the model's behavior velocity vectors are helpful since they enable us to visualize key features of the flux. If anything unexpected happens with the model, then a plan view of vectors or flow paths will easily identify the problem. (Dinh Thanh, Kimura et al. 2010), (Dordevic 2012), (Huang 2000) and (Ramamurthy, Han et al. 2013) have also made this assessment.

Thus, the plan view in Figure 4.1 velocity vector comparison at $z/W = 0.278$ is depicted. Accessing this graph, it becomes apparent that the turbulence model $k-\omega$ SST simulated the general flow behavior correctly. The separation zone is clearly well delimited while the flow particles are concentrated on the right side within the contract region.



Experimental

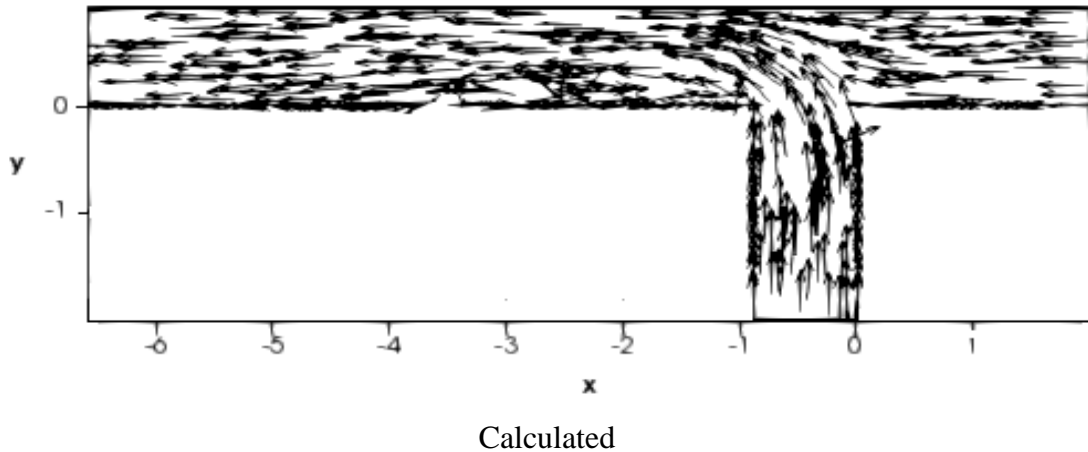


Figure 4.1. Velocity vectors assessment at $z/W = 0.278$

4.2 Longitudinal velocities

In the x direction, the velocity component u is defined which is positive upstream direction. In the majority part of the channel, u velocity is therefore negative, excluding in the zone of separation where the flow is reversed. Next section of this chapter presents the comparison of longitudinal velocity in different forms since the most significant element in the flow is longitudinal velocity.

4.2.1 Comparison of Vertical profiles of Streamwise Velocity

At first hand, the model appears to produce less reliable results. However, to determine the true correctness of a turbulence model a more rigorous review is needed. Figure 4.2 to 4.6 represents the comparison of calculated and experimental data at 6 cross-sections of vertical profiles of longitudinal velocities.

Starting from main channel the cross sections located at $(x/W = 1)$ and $(x/W = 0)$, vertical profiles of streamwise velocities are depicted in Figures 4.2 and 4.3 respectively. x -axis represents the velocity (u) while y -axis represents the depth (z). The values are taken from the bottom of the channel to 0.3m which is the channel mid. The Root Mean Square Error (RMSE) values are also shown in velocity units (i.e., m/s).

The model accurately replicates the shape of the profiles, but they are still lower than the experimental results. Experimental results are twice the numerical results. Figure 2.12 to 2.17 shows that outcomes of this analysis strongly agrees with the findings of (Lira 2014).

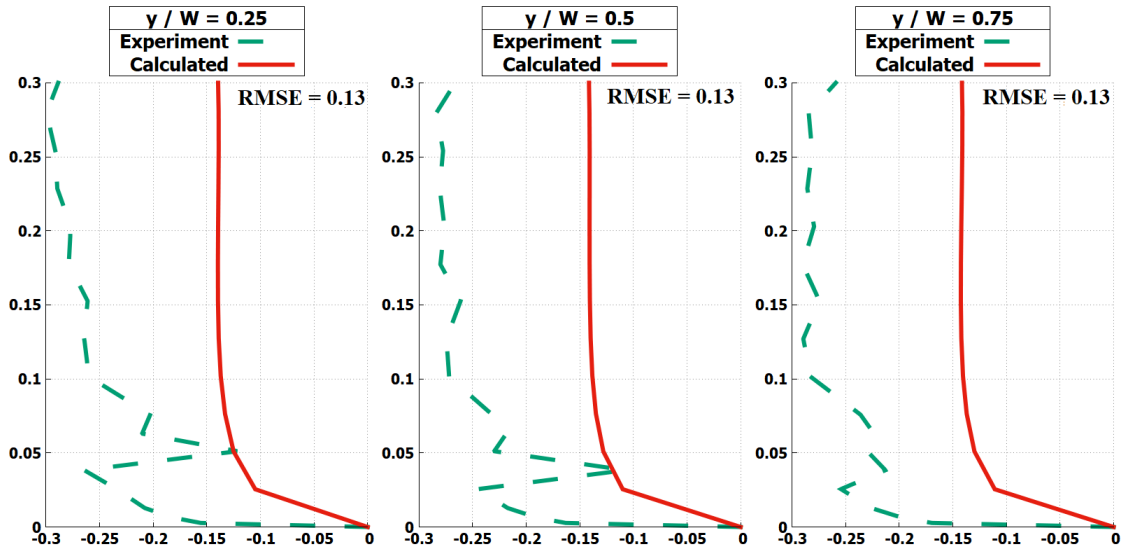


Figure 4.2. Comparison of streamwise velocities at $x/W = 1$

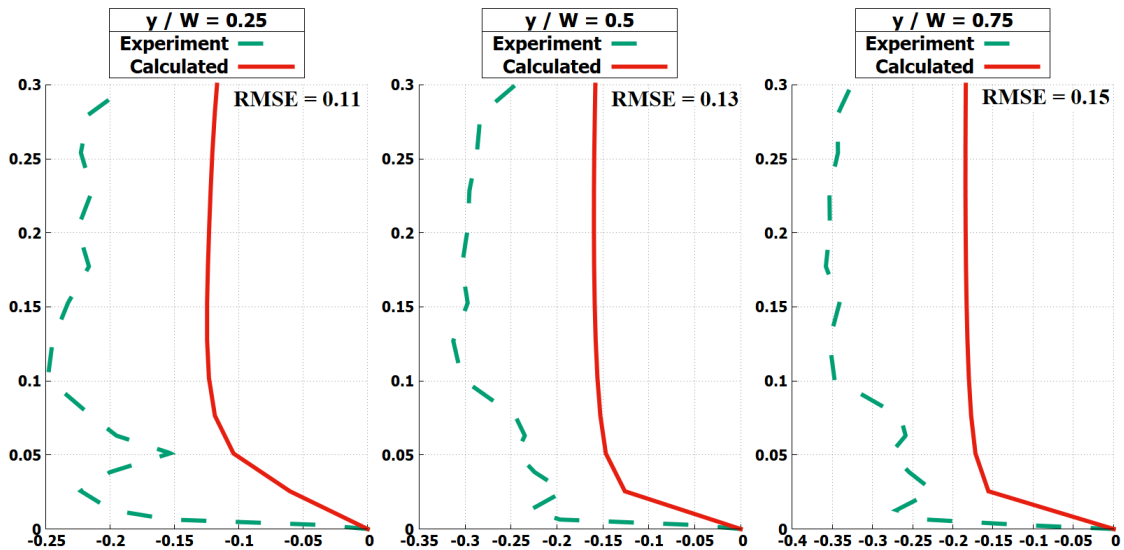


Figure 4.3. Comparison of streamwise velocities at $x/W = 0$

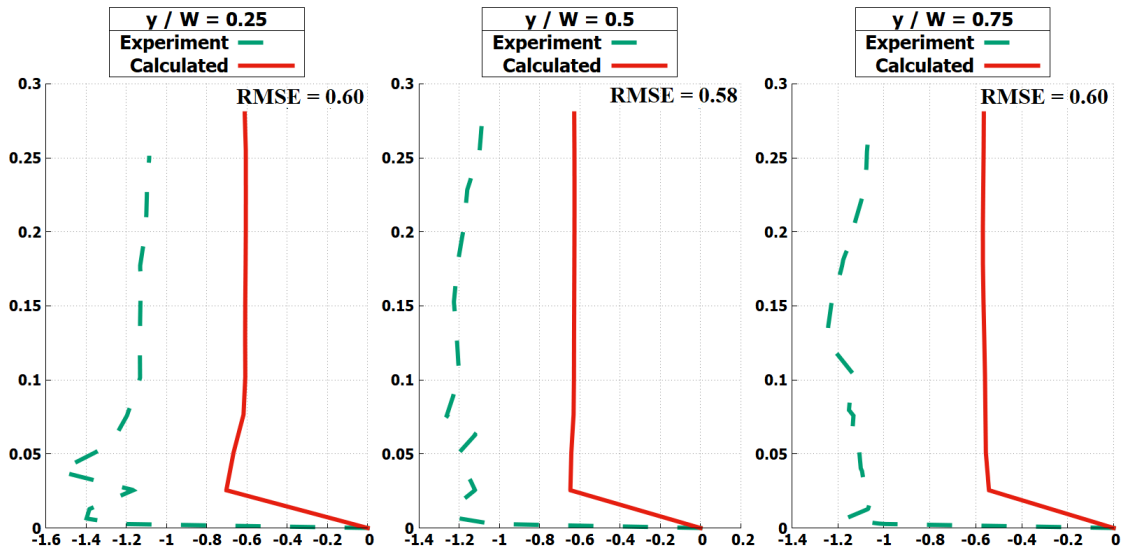


Figure 4.4. Comparison of streamwise velocities at $x/W = -1$

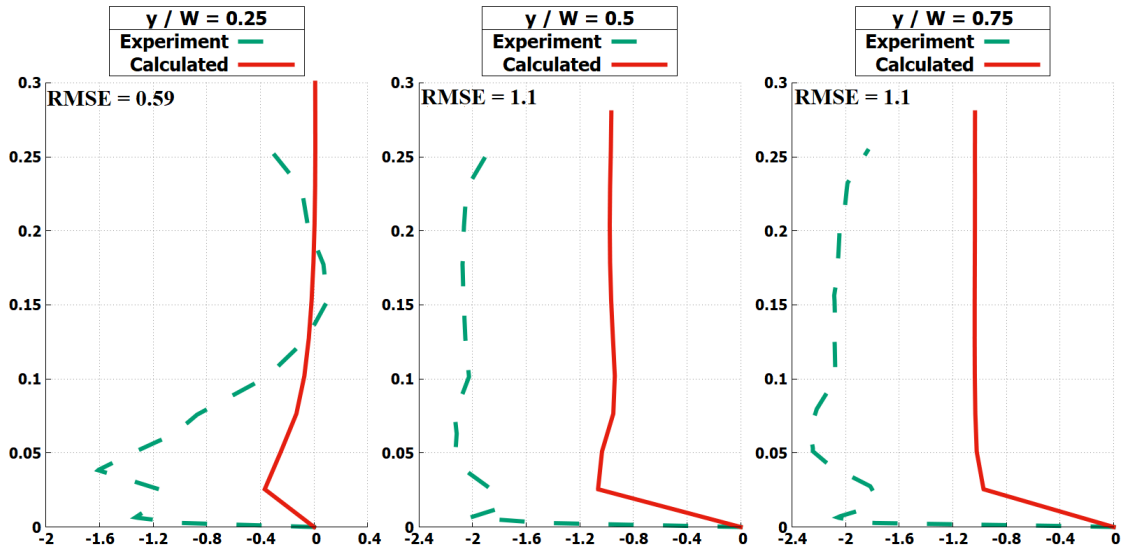


Figure 4.5. Comparison of streamwise velocities at $x/W = -2$

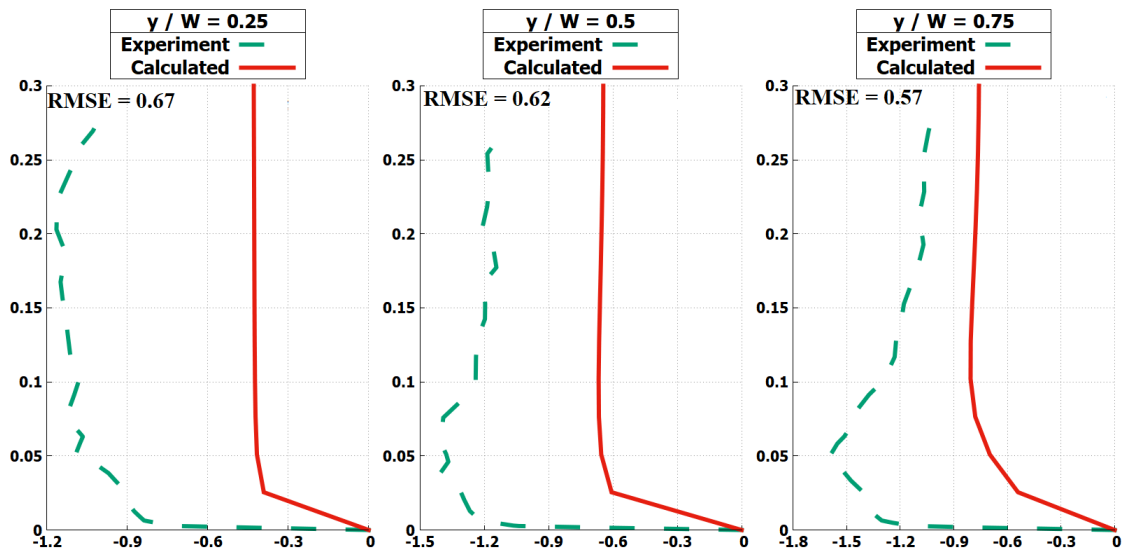


Figure 4.6. Comparison of streamwise velocities at $x/W = -6$

4.2.2 Assessment of velocity variations in plan view

Plan views at two water depths of measured and calculated u velocity contours, $z/W = 0.278$ and $z/W = 0.014$, are shown in Figures 4.7 and 4.8. These plots show dimensionalized velocities, resulting in u^* multiplied by $U_t = u$.

The positive values in red, which characterize the reverse flow, easily identify the separation zone. In Figure 4.7, a contour dash line was drawn to demarcate this area. The maximum widths and lengths were measured and are defined in Table 4-1.

Table 4. 1 Comparison of Separation zone dimensions

Model	Length (m)	Difference (%)	Width (m)	Difference (%)
Experiment	2.15	-	0.25	-
k- ω SST Model	2.2	2.33%	0.2285	8.6%

Experimental findings indicate that the recirculation area seems to disappear near the bottom in figure 4.8. The area near the bottom of higher velocities (in blue) is larger than the area near the surface, according to experiment. The numerical model, however, reveal the reverse with a smaller higher velocity area close to the bottom. In Huang's model, this defect can be identified.

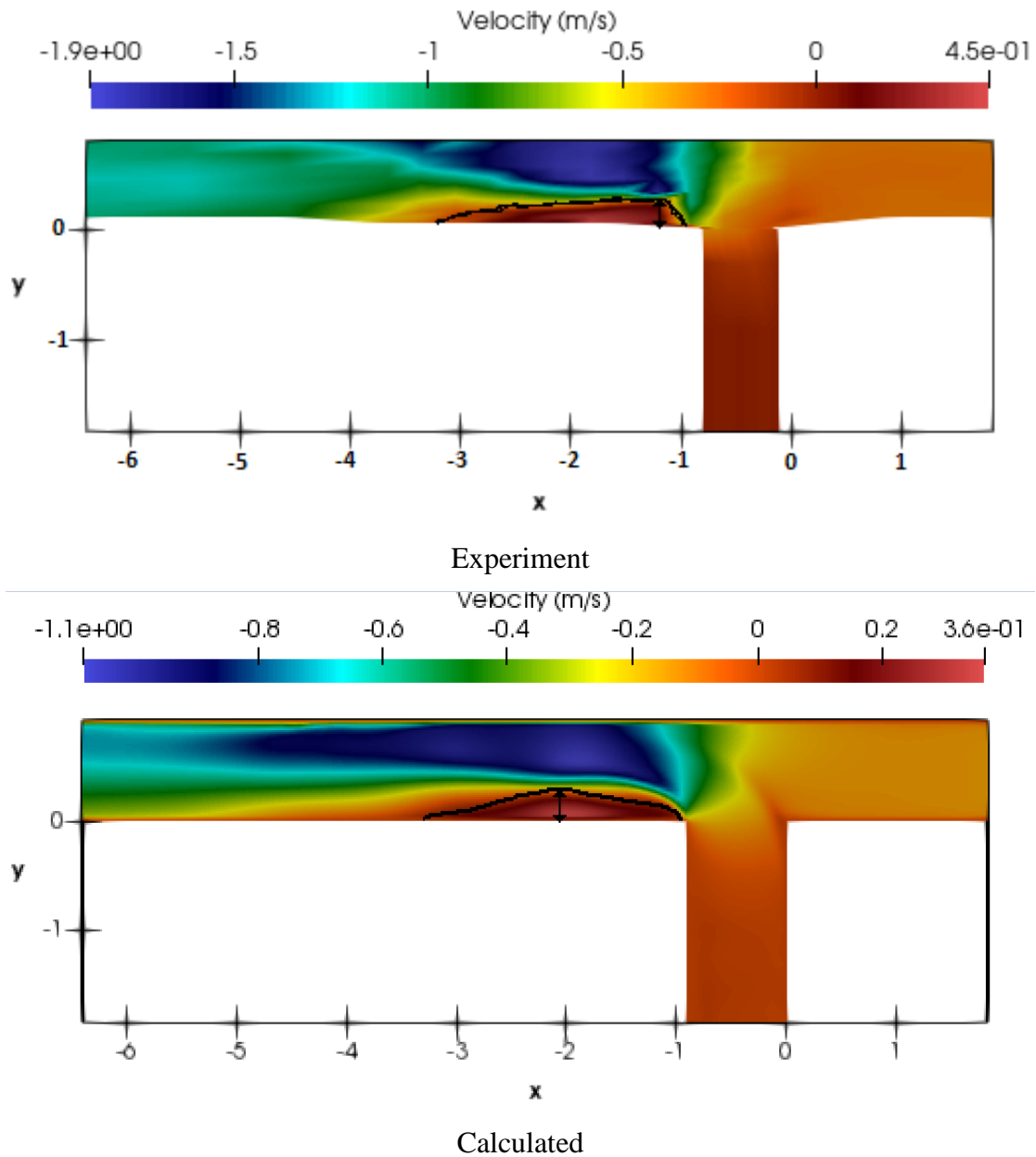
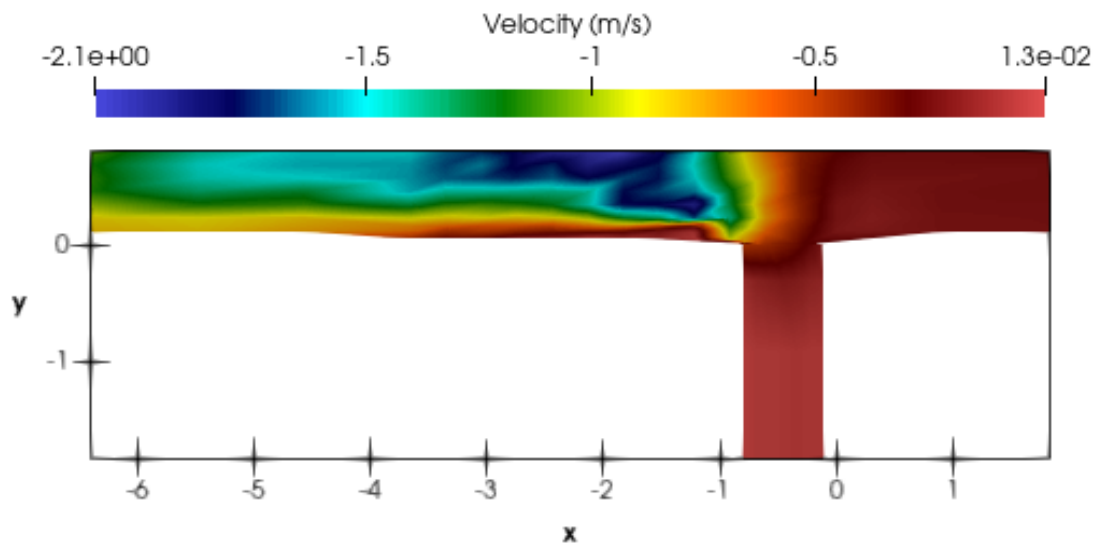
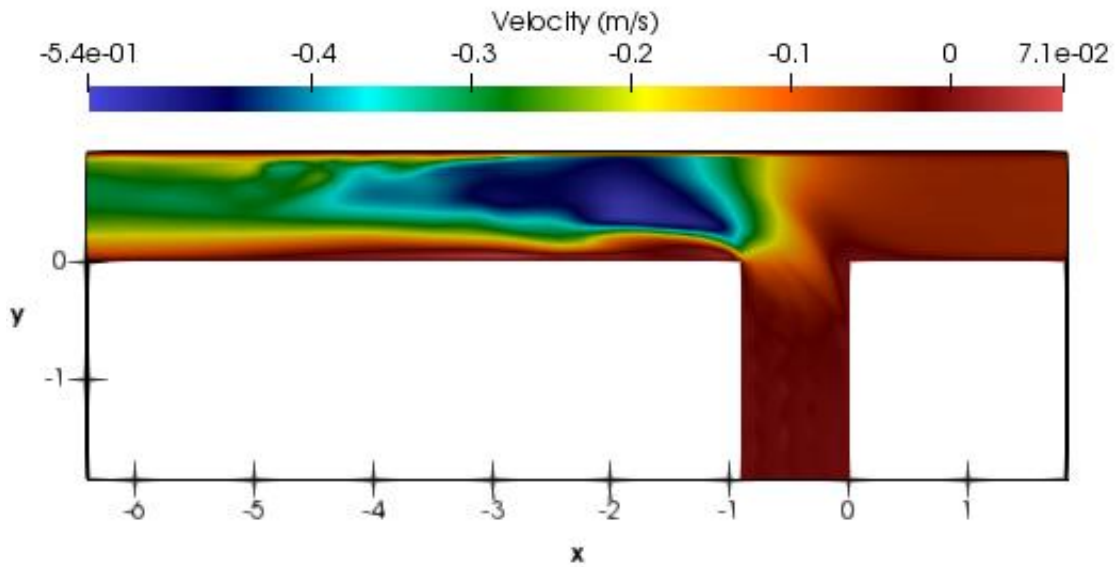


Figure 4.7. Velocity variation assessment at $z/W = 0.278$



Experiment



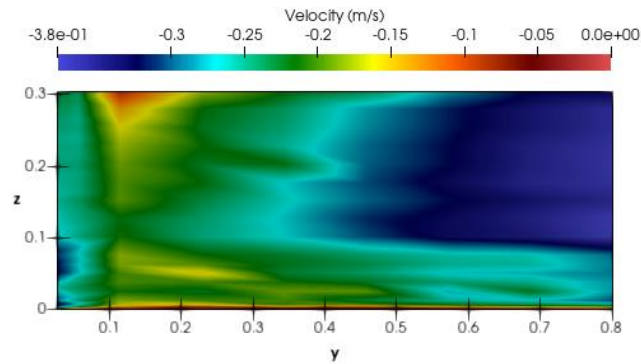
Calculated

Figure 4.8. Velocity variation assessment at $z/W = 0.014$

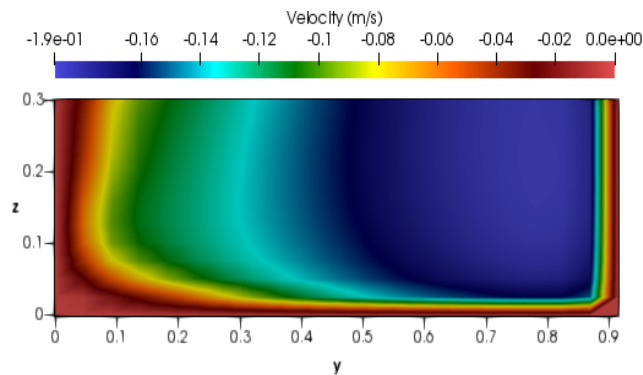
4.2.3 Velocity variation assessment in cross-section

Other comments can be given in cross-sections while focusing on u velocity distributions (Figures 4.9 to 4.12) These plots also display dimensionalized velocities, resulting in u^* multiplied by $U_T = u$.

In cross section $x/W = 0$ the flow begins to migrate right side. (Figure 4.9). This is because of the abundance of flux at the downstream branch channel. It should be noticed that the presence of low (even inverse) velocities on the left side of the main channel indicates a stagnant point at the confluence of an upstream corner.



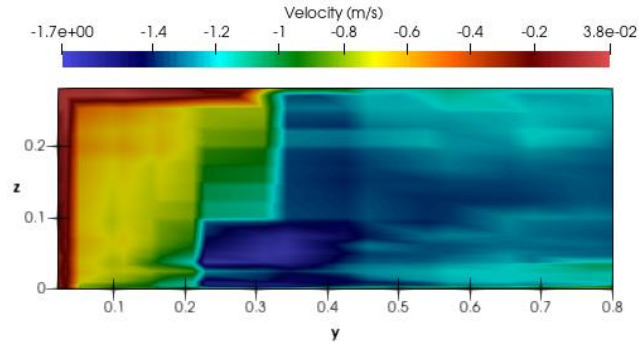
Experiment



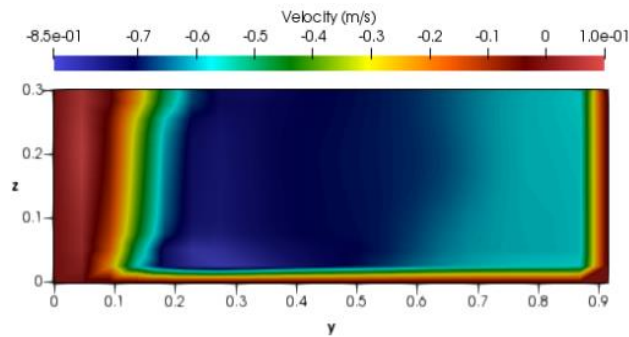
Calculated

Figure 4.9. Velocity variation assessment in cross-section at $x/W = 0$

The flow from both channels is combined at this cross-section $x/W = -1$ in Figure 4.10, and the left wall of the branch channel is in line with the cross section. This segment is at the beginning of the separation zone. The $k-\omega$ SST model defined the u distribution slightly better in this case.



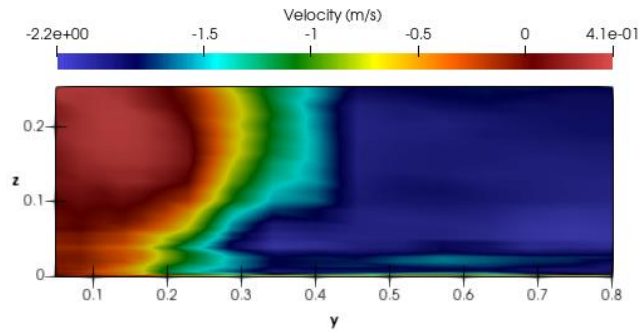
Experiment



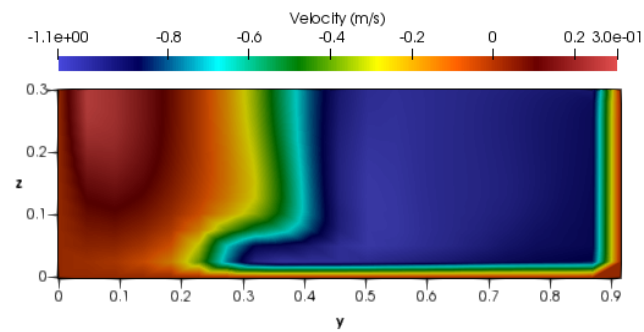
Calculated

Figure 4.10. Velocity variation assessment in cross-section at $x/W = -1$

About $x/W = -1.67$ is the cross-section where the separation zone is greater. Figure 4.11 shows that the numerical models' results are very similar to experimental results.

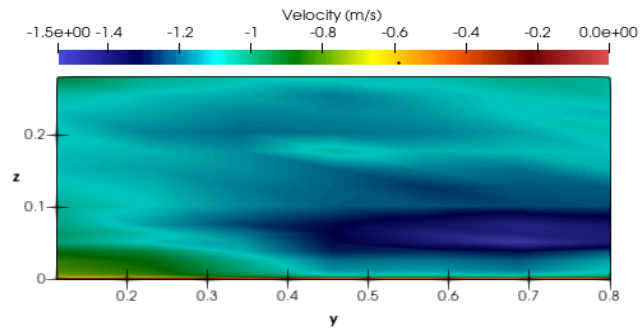


Experiment

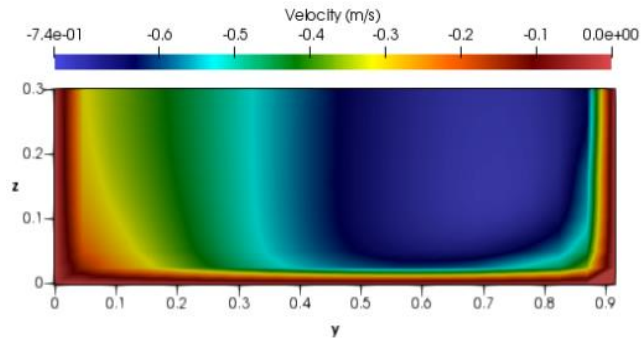


Calculated

Figure 4.11. Velocity variation assessment in cross-section at $x/W = -1.67$. Finally, when the region of higher velocities decreases, velocities at $x/W = -7$ (Figure 4.12) close to the outlet lead to more smooth formed flow. This process happens at a faster rate than it does in computational model. Despite the difficulty of judging, it appears that the $k-\omega$ SST model is closer to the reality of the case.



Experiment



Calculated

Figure 4.12. Velocity variation assessment in cross-section at $x/W = -7$

Above, the experimental results' appearance or contours better fit the numerical model in all situations, but as previously said, the experimental u velocity is twice the numerical results everywhere.

4.3 Free-Surface Treatment

The Rigid-lid approximation was used for the handling of water surfaces by several previous 3D models. While this approach is suitable for some flows, several others have considered it to be inadequate. In (Weber, Schumate et al. 2001), the free-surface elevation shifts dramatically, increasing before and declining after the junction. To examine the velocity distribution neighboring the vicinity of the junction the rigid-lid approximation cannot be accurate. This study therefore suggests that the free surface be more accurately treated. Multiphase flow using an interFoam solver, which captured the variation of the water surface as well, was used for two incompressible, isothermal immiscible fluids using a VOF method. In this parametric analysis, the $k-\omega$ SST model was used as the turbulence model.

4.3.1 Comparison of Water-Surface Elevation

An empirical relationship was established between the number of investigators for the main channel in the upstream section and downstream of the junction for critical depth, which was based on the elevation of the water surface (Hager 1989, Hsu, Lee et al. 1998,

Hsu, Wu et al. 1998, Ramamurthy, Han et al. 2013). Data are not readily available with more depth of surface elevation; however, a 3D numerical model or experimental surface mapping may be used to obtain this information. Figure 4.13 displays the experimental water depth contours and the computed difference in water heights contours (Weber et al, 2001). The depth magnitude is nondimensionalized by tail-water depth (H_0) resulting in z/H_0 . The overall water depth patterns indicate similar trends, as can be seen. The depression downstream of the intersection, as well as the depressions around and around the channels, are visible.

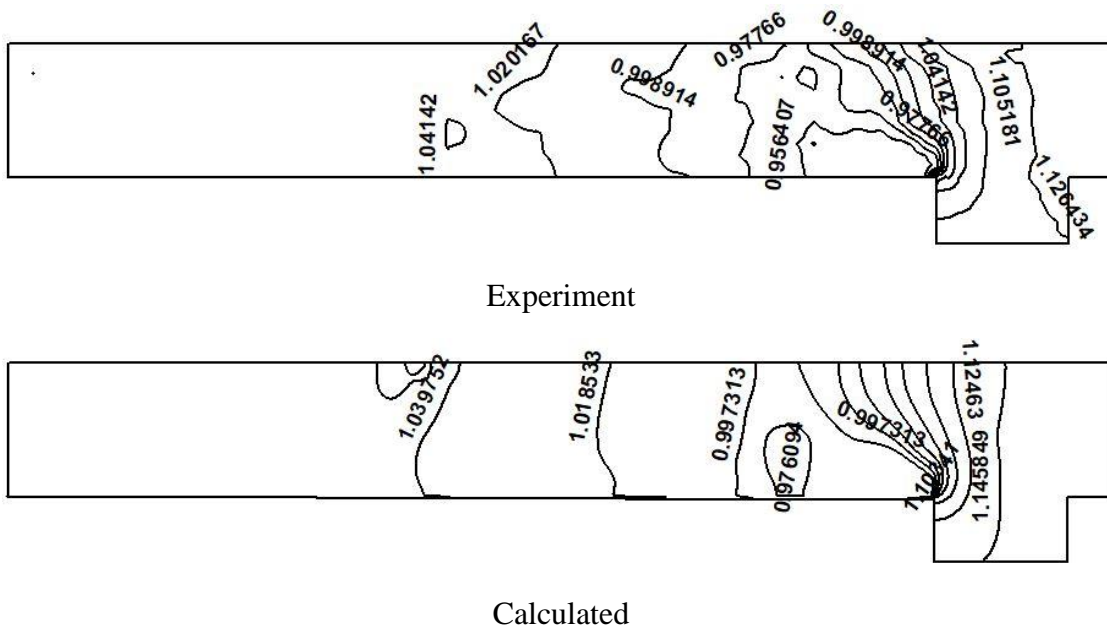
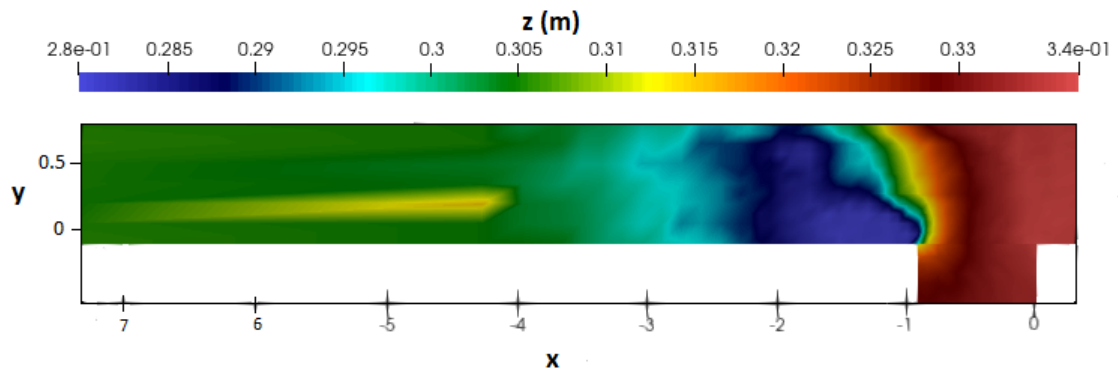
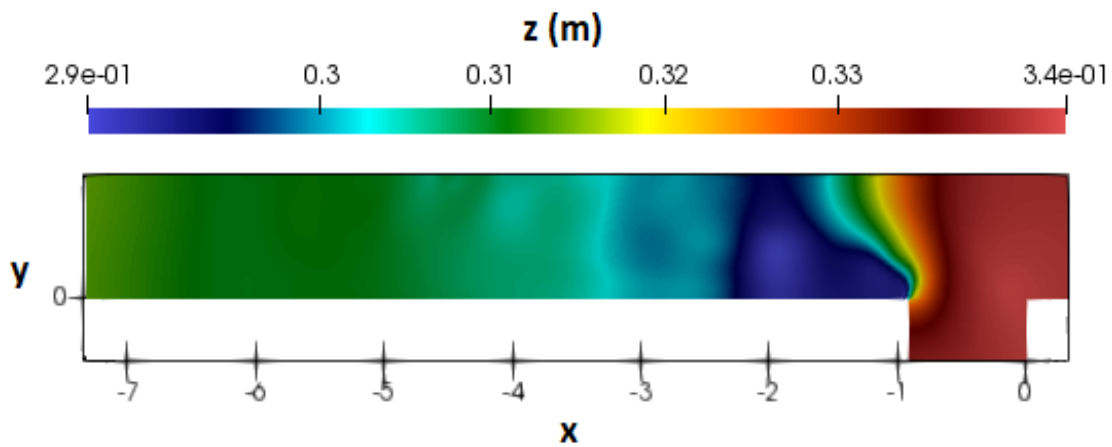


Figure 4.13. Water Surface Contours Comparison

The flow ability of branch channels is increased for low discharge ratio, leading to greater energy loss at the junction. Just behind the junction the flow separates, and the area of separation zone indicates surface depression. The shape of the channel's free surface is accurately replicated. Overall, there is a reasonable and sensible agreement between prediction and experiment.



Experiment



Calculated

Figure 4.14. Water Surface Mapping Comparison

4.3.2 Water surface elevation profiles

In order to make a more quantitative assessment, for this discharge ratio, for seven different z/h values, the simulated and measured water depths were compared. According to existing experimental information, the water surface profile drops just after the confluence. These similarities are shown in Figure 4.15. y -axis represents the nondimensional depth values by dividing the depth of water by the tailwater depth (i.e., 0.296m). The Root Mean Square Error (RMSE) values are also shown having unit of depth. Overall, prediction and experiment have a fair and sensible agreement.

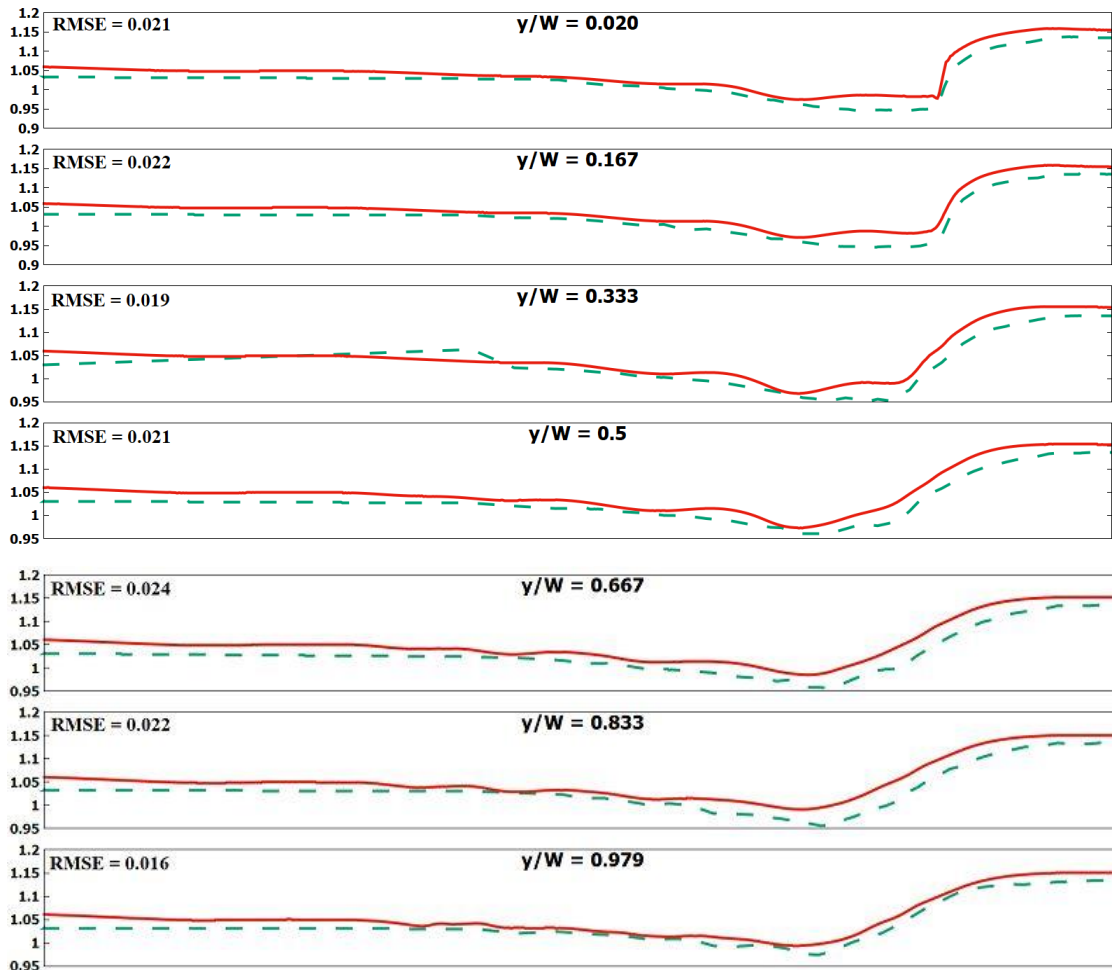


Figure 4.15. Comparison of water surface elevation profiles in the main channel, Green dotted line represent experimental data by (Weber, Schumate et al. 2001) and Red line is present calculation

4.4 Turbulent Kinetic Energy

Figure 4.16 displays the measurement of the turbulent kinetic energy k for near-surface flow for condition $q^* = 0.250$. The higher turbulent area is seen along the border of the moving flow and below the zone of separation. It is worth pointing out that although the side channel flux is affecting the main discharge of the channel, both flows pass through

the channel junction with no overlap. When the rapid velocities of the primary channel flow combine with the decreased velocities of the secondary channel flow, the zone of separation experiences huge turbulence downstream of the junction. TKE had almost the same trend and pattern, which is clear agreement with the experimental findings.

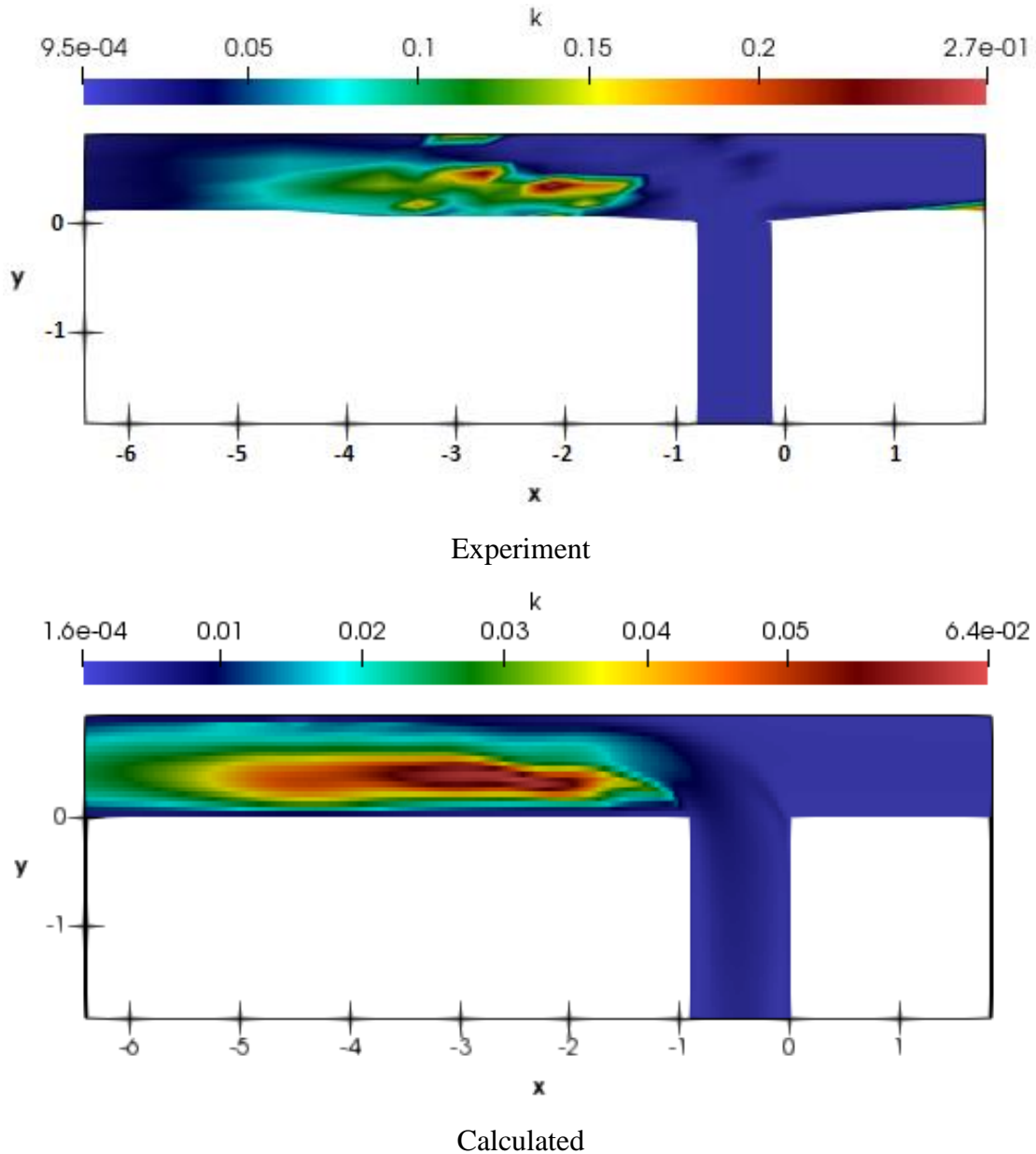


Figure 4.16. Comparison of Turbulent Kinetic Energy at $z/W = 0.278$

CONCLUSIONS AND RECOMMENDATIONS

5.1 Conclusions

Fluid dynamics of a confluence are challenging. On the left of main channel wall downstream of the junction the establishment of a separation zone, in the confluence upstream corner the presence of stagnation point, against the main channel right wall the shock and deflection of the side channel flow, in the contracted region on the right side of the main channel the magnitude of longitudinal velocities is among the difficult flow patterns to model.

A three-dimensional numerical model for a 90° open channel confluence was created in this analysis, and the turbulence model $k-\omega$ SST was tested for $q^* = 0.250$. By comparing the numerical model results to the experimental data, the majority of the flow characteristics were captured at this confluence, thus achieving the primary purpose of this analysis.

Although the overall flow behavior produced by the numerical models is well consistent with the experiment outcomes but there are still several constraints:

- Though the $k-\omega$ SST model was built to be highly effective in terms of replicating eddies and secondary currents, and it did show some ability to illustrate some significant information about the flow current, its magnitude accuracy was weak at most locations. A separation zone occurs immediately downstream of the junction on the left bank. The separation zone was found to be 2.33 percent longer and 8.6 percent wider than in the physical model.
- The $k-\omega$ SST model underpredicts the velocities, as can be seen by looking at the velocity magnitudes.

- Although, in this analysis, we obtained a maximum velocity of 1.2 m/s, whereas the experimental maximum velocity is 2.4 m/s. In comparison to experimental velocity, this model represents magnitudes that are twice as small. However, our findings are very similar to (Lira 2014) and (Huang, Weber et al. 2002) findings.

In comparison with those in the literature, which model the same geometry, the numerical models built here may make the following observations:

- The effect on replication of key flow characteristics at the confluence with CFD Model OpenFOAM was dealt with in this report. No other significant factor was affected apart from the magnitude differences in velocity.
- The findings of water surface mapping and water surface elevation are in strong agreement with those of the experiments.
- The results of the Velocity Vectors produced here agree well with the experiment.
- For modelling two immiscible incompressible fluid-fluid interfaces, volume of fluid (VOF) is an effective and best free-surface method.
- It can be concluded that the accuracy of a numerical model is dependent on a variety of modelling settings and numerical methods.

5.2 Recommendations

In developing this project, the use of OpenFOAM was critical. The investigation suggests further that the programme has a broad range of methods that, when used appropriately, can be very advantageous for modelling numerous flow scenarios. Conversely, due to an inadequacy of interface during the pre-processing phase and an absence of detailed content on the programme tools, this could prevent the individual from building his model accurately and quickly.

Using a 3D model, the current study investigates flow in a T-Shape Channel. It can be improved/refined in the future by

- Using OpenFOAM, compare various turbulence models using VOF method.

- Mesh optimization should be studied and compared between different mesh sizes.
- Different modelling settings and numerical methods can be used.

REFERENCES

Ai, C., et al. (2017). "A hybrid-grid 3D model for regular waves interacting with cylinders." Journal of Hydraulic Research 55(1): 129-134.

Bayon, A., et al. (2016). "Performance assessment of OpenFOAM and FLOW-3D in the numerical modeling of a low Reynolds number hydraulic jump." Environmental Modelling Software 80: 322-335.

Biron, P., et al. (1996). "Effects of bed discordance on flow dynamics at open channel confluences." Journal of Hydraulic Engineering 122(12): 676-682.

Dinh Thanh, M., et al. (2010). "Depth-averaged 2D models with effects of secondary currents for computation of flow at a channel confluence." 137-144.

Dordevic, D. (2012). Application of 3D numerical models in confluence hydrodynamics modeling. 19th international conference on water resources. Urbana-Champaign, June.

Foam, N. (2017). "Boundary Conditions - OpenFOAM-4.1."

Frei, W. (2013). "Which turbulence model should i choose for my cfd application?, 2013." 03-20.

Guide, O. U.-O. F. (2020). "The Open Source CFD Toolbox User Guide."

Gurram, S. K., et al. (1997). "Subcritical junction flow." Journal of Hydraulic Engineering 123(5): 447-455.

Hager, W. H. (1989). "Transitional flow in channel junctions." Journal of Hydraulic Engineering 115(2): 243-259.

Hsu, C.-C., et al. (1998). "Subcritical open-channel junction flow." Journal of Hydraulic Engineering 124(8): 847-855.

Hsu, C.-C., et al. (1998). "Flow at 90 equal-width open-channel junction." Journal of Hydraulic Engineering 124(2): 186-191.

Huang, J. (2000). Development and validation of a three-dimensional numerical model for application to river flow, University of Iowa.

Huang, J., et al. (2002). "Three-dimensional numerical study of flows in open-channel junctions." Journal of Hydraulic Engineering 128(3): 268-280.

Kravchenko, A. G. and P. Moin (2000). "Numerical studies of flow over a circular cylinder at $Re_D = 3900$." Physics of Fluids 12(2): 403-417.

Lira, V. M. P. (2014). "Numerical modeling of a 90° openchannel confluence flow using openfoam CFD."

Mamedov, A. S. (1989). "Hydraulic calculation of a confluence." Hydrotechnical construction 23(9): 553-556.

Menter, F. R. (1994). "Two-equation eddy-viscosity turbulence models for engineering applications." AIAA journal 32(8): 1598-1605.

OpenFOAM, O. U. G. (2014). OpenFOAM Foundation, February.

Ramamurthy, A., et al. (2013). "Three-dimensional simulation parameters for 90 open channel bend flows." Journal of Computing in Civil Engineering 27(3): 282-291.

Schlichting, H. (1979). "Boundary Layer Theory, 7th McGraw-Hill." New York.

Shabayek, S., et al. (2002). "Dynamic model for subcritical combining flows in channel junctions." Journal of Hydraulic Engineering 128(9): 821-828.

Taylor, E. H. (1944). "Flow characteristics at rectangular open-channel junctions." ASCE 109(1): 893-902.

Versteeg, H. K. and W. Malalasekera (2007). An introduction to computational fluid dynamics: the finite volume method, Pearson education.

Vu, H. C., et al. (2016). "Numerical investigation of flow around circular cylinder with splitter plate." KSCE Journal of Civil Engineering 20(6): 2559-2568.

Webber, N. B. and C. Greated (1966). "An investigation of flow behaviour at the junction of rectangular channels." Proceedings of the Institution of Civil Engineers 34(3): 321-334.

Weber, L. J., et al. (2001). "Experiments on flow at a 90 open-channel junction." Journal of Hydraulic Engineering 127(5): 340-350.

White, F. M. and I. Corfield (2006). Viscous fluid flow, McGraw-Hill New York.